# The Investigation of Tumor-on-a-Chip via 3D-Bioprinting Methods

## Master Thesis

For the attainment of the academic degree

**Master of Science**

From the University of Applied Sciences FH Campus Wien


**Submitted by:**
Matthias Vostatek, BSc

**Personal identity code**
C1810544013

**Supervisor:**
Yu Shrike Zhang, PhD
Brigham and Women's Hospital – Harvard Medical School
Cambridge
USA


**Submitted on:**
17. 02. 2021

## Abstract

Cancer is with rising prevalence the worldwide second leading cause of mortality after cardiovascular diseases. Hence, cancer is a severe problem which affects the health of societies around the globe. Cholangiocarcinoma is a diverse rare epithelial tumor with increasing incidence worldwide and an aggressive tumor with poor prognosis. Therefore, various efforts are being directed to the search for an appropriate drug screening model. At the moment, cholangiocarcinoma models include a variety of mouse models: genetically engineered, carcinogen-induced and xenotransplants of cholangiocarcinoma. Another promising model uses patient-derived cholangiocarcinoma organoids. In principle, mouse models are reproducible and can be monitored easily. Nevertheless, they are difficult to operate and have many predictive problems as seen in other animal models. Patient-derived organoids are simpler to handle and do not have the problem of species mismatch. However, they lack perfusion. Tumor-on-a-chip systems are a hopeful alternative. They are able to mimic the tumor microenvironment, add high-throughput drug screening possibilities, and redress the ethical concerns of animal testing.

As the established drug testing methods for cholangiocarcinoma have their disadvantages and the tumor-on-a-chip systems display promising features, the aim of the project was to fabricate a 3D cholangiocarcinoma-on-a-chip which closely mimics the *in vivo* counterpart. The chip consists of cholangiocarcinoma, hepatic and vessel cells. The chips were produced manually via photo-initiated GelMA, as well as through 3D bioprinting. When compared to 2D monoculture, the 3D cholangiocarcinoma-on-a-chip displayed many upregulated genes in cancer pathways, such as the p53 pathway. Further screenings also showed more sensitivity to an antitumor prodrug, due to biotransformation capabilities of neighboring hepatic cells in the cholangiocarcinoma-on-a-chip model. Overall, the findings of this master thesis project point out that cholangiocarcinoma-on-a-chip is a promising drug screening tool and possible option for personalized medicine. Also, it could be seen that this novel model can be produced in high quality, with little human input, and in a short amount of time.

## Abstract (German)

Die zweithäufigste Todesursache weltweit, nach Herz-Kreislauf-Erkrankungen, ist Krebs mit ständig steigender Prävalenz. Cholangiokarzinom ist ein vielfältiger, seltener und aggressiver epithelialer Tumor mit weltweit zunehmender Inzidenz und schlechter Prognose. Daher wird viel Augenmerk auf die Suche nach einem geeigneten Arzneimittel-Screening-Modell gerichtet. Derzeit umfassen Cholangiokarzinom-Modelle eine Vielzahl von Mausmodellen: gentechnisch veränderte, Krebs induzierte und Xenotransplantate des Cholangiokarzinoms. Ein weiteres vielversprechendes Modell verwendet von Patienten stammende Cholangiokarzinom-Organoide. Im Prinzip sind Mausmodelle reproduzierbar und leicht überwachbar. Sie sind jedoch schwierig handzuhaben und weisen viele Vorhersageprobleme auf, wie es auch bei anderen Tiermodellen der Fall ist. Von Patienten stammende Organoide sind einfacher handzuhaben und haben nicht das Problem, dass die Spezies nicht dieselbe ist. Es fehlt ihnen jedoch die Perfusion. Tumor-on-a-chip Systeme sind eine hoffnungsvolle Alternative. Sie sind in der Lage, die Tumor-Mikroumgebung nachzuahmen, Möglichkeiten für das Wirkstoff-Screening mit hohem Durchsatz durchzuführen und die ethischen Bedenken von Tierversuchen zu umgehen.

Da die etablierten Drogentestmethoden für Cholangiokarzinome ihre Nachteile mit sich ziehen und die Tumor-on-a-chip Systeme vielversprechende Merkmale aufweisen, bestand das Ziel dieses Masterprojektes darin, ein 3D-Cholangiokarzinom-on-a-chip herzustellen, welches das *in vivo* Gegenstück nachahmt. Der Chip besteht aus Cholangiokarzinom-, Leber-, und Gefäßzellen. Die Chips wurden hergestellt mittels photoinitiiertem GelMA, sowohl manuell als auch durch 3D-Biodrucken. Im Vergleich zur 2D-Monokultur zeigte das 3D Cholangiokarzinom-on-a-chip viele hochregulierte Gene in Krebspfaden, wie dem p53-Pfad. Weitere Untersuchungen zeigten auch eine höhere Empfindlichkeit gegenüber einem Antitumor-Prodrug aufgrund der Biotransformationsfähigkeit benachbarter Leberzellen im Cholangiokarzinom-on-a-chip Modell. Alles in allem zeigen die Ergebnisse dieses Masterarbeitsprojektes, dass das Cholangiokarzinom-on-a-chip ein vielversprechendes Werkzeug für das Wirkstoff-Screening und eine mögliche Option für die personalisierte Medizin darstellt. Es konnte ebenfalls festgestellt werden, dass dieses neuartige Modell in hoher Qualität, mit wenig Aufwand und in kurzer Zeit hergestellt werden kann.

## Key terms

DMD bioprinting,
gelatin methacryloyl,
cholangiocarcinoma,
tumor-on-a-chip,
drug screening

## Preface

The following thesis is going to sum up the experience of the Master internship in the 4th and 5th semester of FH Campus Vienna's Master program "Molecular Biotechnology", which lasted from February 2020 until December 2020. The work was performed under the supervision of the group of Yu Shrike Zhang, PhD at the Brigham and Women's Hospital, which is part of the Harvard Medical School. Due to the worldwide COVID-19 pandemic, the internship was paused between mid-March and mid-August. The internship was financially supported by the Austrian Marshall Plan Foundation.

## Table of Contents

## List of Abbreviations

| | |
|---|---|
| % | Percent |
| 2D | Two-dimensional |
| 3D | Three-dimensional |
| BSA | Bovine serum albumin |
| CCA | Cholangiocarcinoma |
| CD | Cluster of differentiation |
| cfDNA | Cell free DNA |
| CK | Cytokeratin |
| $CO_2$ | Carbon dioxide |
| CTCs | Circulating tumor cells |
| CYP450 | Cytochrome P450 |
| DAPI | 4′,6-Diamidin-2-phenylindol, |
| dCCA | Distal Cholangiocarcinoma |
| DLP | Digital light processing |
| DMD | Digital micromirror device |
| DNA | Desoxyribonucleic acid |
| DOD | Drop-on-demand |
| DPBS | Dulbecco's phosphate-buffered saline |
| eCCA | Extrahepatic Cholangiocarcinoma |
| ECM | Extracellular matrix |

| | |
|---|---|
| EGFP | Enhanced green fluorescent protein |
| EGFR | Epidermal growth factor receptor |
| FBS | Fetal bovine serum |
| GelMA | Gelatin methacryloyl |
| GFP | Green-fluorescent protein |
| h | Hours |
| HCC | Hepatocellular carcinoma |
| Hep-G2 | Liver cancer cell line |
| HGT | Horizontal gene transfer |
| HUVEC | Human umbilical vein endothelial cell |
| iCCA | Intrahepatic cholangiocarcinoma |
| Ig | Immunoglobulin |
| LAB | Laser-assisted bioprinting |
| MDR | Multi-drug-resistance |
| min | Minutes |
| NCI | National Cancer Institute |
| o/n | Overnight |
| Pa | Pascal |
| PBS | Phosphate-buffered saline |
| pCCA | Perihilar cholangiocarcinoma |
| PDMS | Polydimethylsiloxane |

| | |
|---|---|
| PFA | Para formaldehyde |
| PI | Photoinitiator |
| PMMA | Poly(methacrylic acid) |
| RBE | Cholangiocarcinoma cell line |
| RFP | Red fluorescent protein |
| RNA | Ribonucleic acid |
| RNA-seq | RNA-sequencing |
| rpm | Rounds per minute |
| RU | Ruthenium |
| s | Seconds |
| SPS | Sodium persulfate |
| SLA | Stereolithography |
| TME | Tumor microenvironment |
| UV | Ultraviolet |
| VEGF | Vascular endothelial growth factor |
| wt./vol | Weight to volume |

## List of Figures

## List of Tables

# 1. INTRODUCTION

## 1.1 Cancer

Cancer is with rising prevalence the worldwide second leading cause of mortality after cardiovascular diseases (Nagai & Kim, 2017). In the US alone, around 1,665,540 humans suffered from cancer, and 585,720 of these died from cancer by 2014 (Hassanpour & Dehghani, 2017; R. Siegel, Naishadham, & Jemal, 2013). Hence, cancer is a severe problem which affects the health of societies around the globe. Unfortunately, at the tissue level, it is a variable disease and this variety is a key challenge for the specific diagnosis and treatment efficacy (Fisher, Pusztai, & Swanton, 2013; Hassanpour & Dehghani, 2017; Meacham & Morrison, 2013). The highest percentages of cancer in men develop in the prostate, bronchus and lung, rectum and colon, and urinary bladder, respectively. Cancer prevalence in women is the highest in breast, bronchus and lung, rectum and colon, uterine corpus and thyroid, respectively. This data demonstrates that breast and prostate cancer comprise a major portion of cancer in women and men, respectively (Hassanpour & Dehghani, 2017; R. L. Siegel, Miller, & Jemal, 2016). The highest percentage of cancer in children are blood cancers, and brain and lymph node related cancers, respectively (Hassanpour & Dehghani, 2017; Schottenfeld & Fraumeni Jr, 2006; Yoo & Shin, 2003).

Cancer establishes due to a series of consecutive gene mutations which eventually lead to changes in cell functions. Chemical compounds have an obvious role in causing gene mutations and successive development of cancer cells. For example, smoking is associated with several carcinogenic compounds which can lead to lung cancer (Aizawa et al., 2016; Hassanpour & Dehghani, 2017). Environmental chemical compounds can also have carcinogenic properties and have a direct or indirect influence on the nucleus and cytoplasm of cells, which could lead to gene mutations and genetic disorders (Antwi et al., 2015; Cumberbatch, Cox, Teare, & Catto, 2015; Hassanpour & Dehghani, 2017; Poon, McPherson, Tan, Teh, & Rozen, 2014; Trafialek & Kolanowski, 2014). Radiation, bacteria and viruses are additional carcinogenic factors, which constitute about seven percent of all cancers (Hassanpour & Dehghani, 2017; Parkin, 2006). Generally, cancer disturbs cellular relations and leads to dysfunction of vital genes. This disruption is effective in the cell cycle, and results in abnormal proliferation (Cigudosa et al., 1999; Hassanpour & Dehghani, 2017; Seto, Honma, & Nakagawa, 2010). Under normal conditions, cell division and growth are governed by proto-oncogenes, but these become oncogenes when undergoing genetic

mutation, which is threatening cell existence (Hassanpour & Dehghani, 2017; Shtivelman, Lifshitz, Gale, & Canaani, 1985). Additionally, uncontrolled cell division is triggered by the lack of tumor suppressor genes (Hassanpour & Dehghani, 2017; Matlashewski et al., 1984). Usually, repair genes are translated into enzymes and proteins which have repairing properties. There are over 30 types of detected repair proteins (Hassanpour & Dehghani, 2017; Qingyi & Lei, 2007). The DNA damage, induced by ultraviolet (UV) light, for example, is bypassed by removing uracil, which removes the main DNA lesions. Essentially, this function of repair proteins leads to successful repair of DNA and defects in these repair mechanism can lead to cancer (Hassanpour & Dehghani, 2017; Wood, Mitchell, & Lindahl, 2005).

### 1.1.1 Cholangiocarcinoma

Cholangiocarcinoma (CCA) comprises an assorted group of malignancies coming from the biliary tree (Figure 1). CCAs are divided into three subgroups depending on the site of origin: distal (dCCA), perihilar (pCCA), and intrahepatic (iCCA) CAA (Jesus M Banales et al., 2016; Jesus M. Banales et al., 2020; Rizvi, Khan, Hallemeier, Kelley, & Gores, 2018).

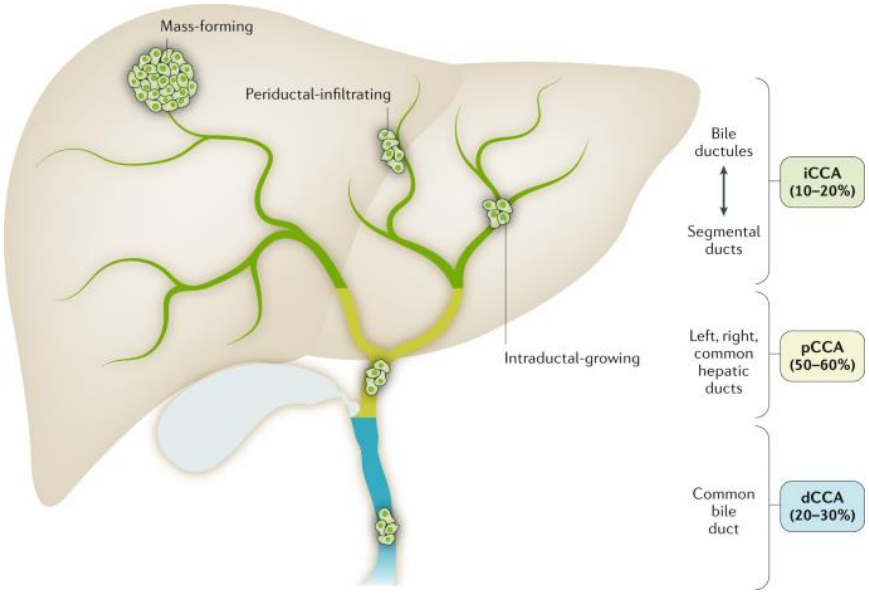


Figure 1: Classification of cholangiocarcinoma. According to the anatomical site of origin, CCA is divided into distal (dCCA), perihilar (pCAA), and intrahepatic (iCCA) CCA. dCCA is located at the common bile duct, pCCA involves the left and/or right hepatic duct and/or their junction, and iCCA arises as a malignancy in the periphery of the second-order bile ducts. Roughly, CCA can display three main growth patterns: mass-forming, periductal-infiltrating, and intraductal-growing. Mass-forming CCA exists as a mass lesion in the hepatic parenchyma. Periductal-infiltrating builds inside the duct wall and expands along the wall longitudinally. Intraductal-growing CCA exists as papillary or polypoid tumor and grows towards the duct lumen. Image from (Jesus M. Banales et al., 2020).

Noteworthy, a mixed type of hepatocellular carcinoma (HCC) and cholangiocarcinoma exists, which is a rare type of liver malignancy sharing traits of both HCC and iCCA, and poses an aggressive disease course and poor prognosis (Jesus M. Banales et al., 2020; Brunt et al., 2018; Munoz-Garrido & Rodrigues, 2019). iCCA emerges above the second-order bile ducts, whereas the insertions of the cystic duct can be taken as anatomical distinction point between pCCA and dCCA. Both can collectively also be referred to as extrahepatic CCA (eCCA) (Jesus M. Banales et al., 2020; Khan & Dageforde, 2019). pCCA is—in the United States—the most commonly found, accounting for approximately 50 to 60% of all CCA cases, followed by dCCA with around 20 to 30%, and last iCCA with 10 to 20% (Jesus M Banales et al., 2016; Jesus M. Banales et al., 2020; DeOliveira et al., 2007; Nakeeb et al., 1996). CCA is the second most common primary hepatic malignancy after HCC, comprising around 15% of all primary liver tumors and three percent of gastrointestinal tumors (Jesus M Banales et al., 2016; Jesus M. Banales et al., 2020; DeOliveira et al., 2007; Nakeeb et al., 1996). Due to being mostly asymptomatic in early stages, CCA is often diagnosed only in advanced stages, which highly compromises the available therapeutic options, resulting in a poor prognosis (Andersen et al., 2012; Jesus M Banales et al., 2016; Jesus M. Banales et al., 2020).

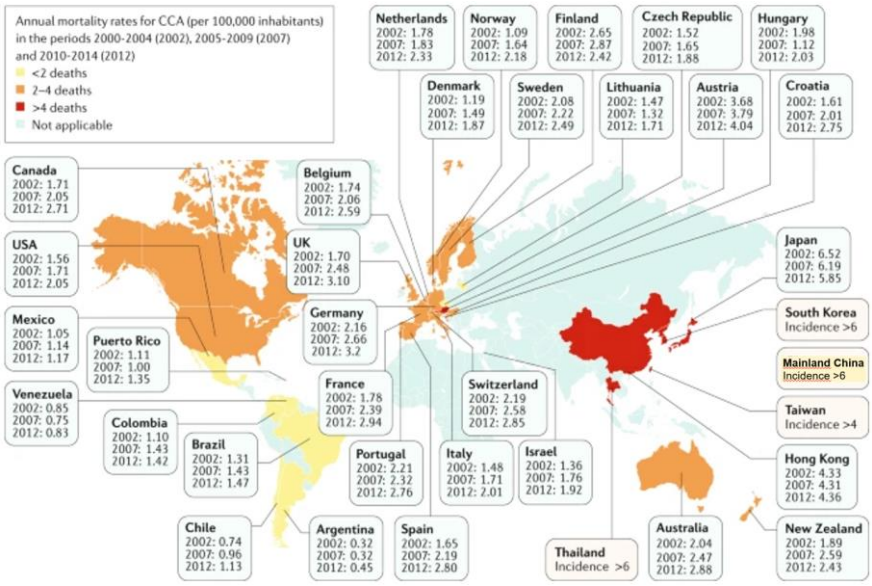


Figure 2. Worldwide mortality of cholangiocarcinoma. Global annual mortality rates for CCA (deaths per 100,000 inhabitants). Yellow shows low mortality (<2 deaths per 100,000), orange shows medium mortality (2–4 deaths per 100,000) and red shows high mortality (>4 deaths per 100,000). Mortality of the eastern region, including Thailand, China and South Korea, have not been reported and therefore, incidence is shown for this region. Data from the time periods 2000–2004 (2002), 2005–2009 (2007), and 2010–2014 (2012). Image from (Jesus M. Banales et al., 2020).

CCA is a comparatively rare cancer, however with rising incidence and mortality worldwide in the past few decades, therefore representing a global health problem as can be seen in Figure 2. In spite of advances in CCA knowledge, awareness and therapies, prognosis for patients has not substantially improved in the recent years, with five year survival and tumor recurrence rates after removal still being grim (Alabraba et al., 2019; Jesus M. Banales et al., 2020; Kamsa-ard et al., 2020; Koerkamp et al., 2015; Komaya et al., 2018; Lindnér, Rizell, & Hafström, 2015; Strijker et al., 2019). Consequently, thorough studies have to be conducted on these types of cancers to improve patient outcomes and welfare.

### 1.1.2 Tumor microenvironment

The tumor formation and progression process are generally influenced by two main factors, namely changes in genetics/epigenetics of the tumor cells and the disturbance of tumor microenvironment (TME) components through mutual and dynamic crosstalk (Baghban et al., 2020; Jahanban-Esfahlan, Seidi, Monhemi, et al., 2017). The tumor microenvironment consists of tumor cells, stromal cells of the tumor—including endothelial cells and stromal fibroblasts—and immune cells such as macrophages, lymphocytes, and microglia (Figure 3). Additionally, there are also non-cellular elements of the extracellular matrix such as fibronectin, collagen, laminin, hyaluronan, and many more (Baghban et al., 2020; Jahanban-Esfahlan, Seidi, & Zarghami, 2017; Jahanban-Esfahlan, Seidi, Banimohamad-Shotorbani, Jahanban-Esfahlan, & Yousefi, 2018). At the heart of the TME lie the tumor cells which control the behavior of cellular and non-cellular elements through intricate signaling networks to utilize the non-malignant cells for their own benefit. The result of these crosstalks can be seen in tumor formation and maintenance as well as multi-drug-resistance (MDR) and inadequate response to therapies. The non-malignant cells within the TME have been established to promote tumorigenesis in all phases of development and metastasis of cancer (Baghban et al., 2020; Frisch, Angenendt, Hoth, Prates Roma, & Lis, 2019; Hanahan & Coussens, 2012).

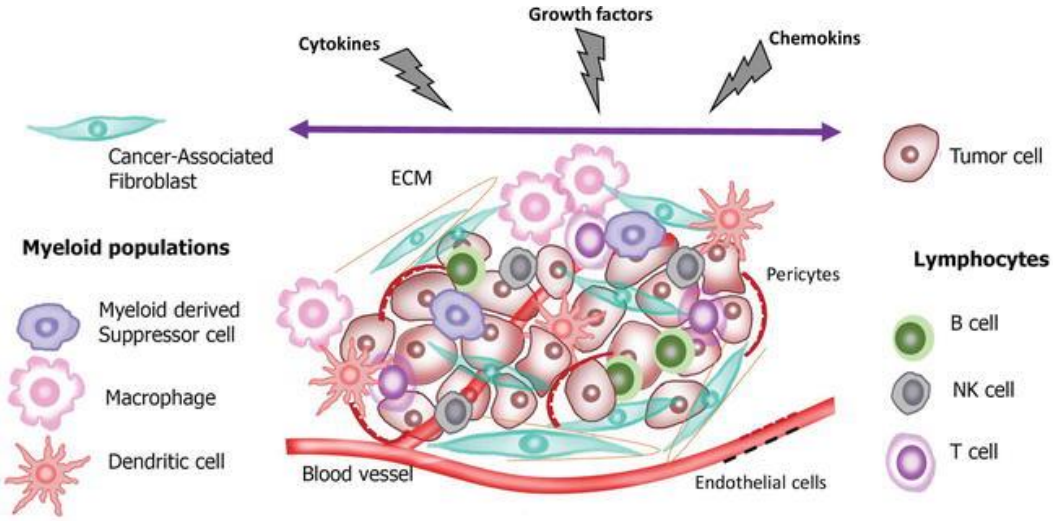


Figure 3 Tumor microenvironment. Image from (Alsibai & Meseure, 2018)

The intercellular communication derives from an intricate network of growth factors, chemokines, cytokines, matrix remodeling enzymes and inflammatory mediators, but also other riveting mechanisms of interaction come to light in recent years. These include cell-free DNA (cfDNA), exosomes, circulating tumor cells (CTCs), and apoptotic bodies as new horizontal gene transfer (HGT) mediators originating from tumor cells and conveying information to target cells including healthy and/or tumor cells (Baghban et al., 2020; Denisenko, Budkevich, & Zhivotovsky, 2018). Recent progress in studies regarding tumor biology have demonstrated that it is essential to analyze the multiple exchanges between the tumor cells and their surrounding TME, and therefore understanding the various underlying mechanisms of metastasis and tumor growth (Baghban et al., 2020; Jahanban-Esfahlan, de la Guardia, Ahmadi, & Yousefi, 2018). The loss of carcinogenesis, further progress and tissue integrity appears as a consequence of alternate interactions between tumor cells with the extracellular matrix (ECM) and the TMEs cellular components (Baghban et al., 2020; Jahanban-Esfahlan et al., 2019; Seidi, Neubauer, Moriggl, Jahanban-Esfahlan, & Javaheri, 2018).

Owing to the imperative role of the TME in malignancy, diverse efforts are focused on this area (Oliver et al., 2018; Sounni & Noel, 2013). This better perception of the course in which cancer progression is affected by the TME, can make new targets available for cancer treatment. This can be accomplished by interrupting the intricate crosstalk between cancer cells, non-malignant cells and the surrounding ECM (Baghban et al., 2020; Seidi et al., 2018).

Thus, the simulation of TME is a crucial challenge in the development of novel cancer models. In order to establish a reliable model for drug development and personalized cancer therapy, it is of most importance to preserve the original tumor's key features. In recent years, advances have been made in three-dimensional platforms through microfluidic devices, which bring immense opportunity to better simulate the TMEs biology and function, and overcome the gap between preclinic and clinic research (Ayoubi-Joshaghani et al., 2020; Baghban et al., 2020; Sleeboom, Amirabadi, Nair, Sahlgren, & Den Toonder, 2018).

## 1.2 Anti-tumor drug screening

*In vitro* models are a crucial tool in the search for new anti-tumor drugs and assessing the effectiveness of such. Tumor models, when authentic, enable a more comprehensive screening of potential drugs against tumors and hence prevent insufficient drugs from entering the preclinical phase of animal testing. Pharmacological testing in animal models is carried out to evaluate toxicity, bioavailability, and therapeutic efficacy at certain doses (Kristina V. Kitaeva, Rutland, Rizvanov, & Solovyeva, 2020; Stevens & Baker, 2009). According to industry standards, all novel drugs are obligated to undergo preclinical trials with animal models before being admitted to clinical trials in humans. Nevertheless, using animal models has some disadvantages including differential responses due to species variations, high costs, and limitations in test feasibility and availability (Bileckot et al., 1991; Kristina V. Kitaeva et al., 2020). This introduces a requirement and opportunity to create more modern *in vitro* models to determine the therapeutic efficacy of drugs (Kristina V. Kitaeva et al., 2020). A quick overview of advantages, disadvantages and application of the various tumor models can be seen in Table 1.

Table 1. Comparison of various cell culture systems used for anticancer drug screening (Kristina V. Kitaeva et al., 2020)

| Tumor model | Advantages | Disadvantages | Application |
|---|---|---|---|
| **2D model** | Simple; cost-effective; multiple compound libraries possible | No complex 3D tissue architecture; no interaction with TME or ECM or other cells | Anticancer drug screening |
| **3D spheroids** | Able to reproduce intercellular and paracrine interaction; complex 3D architecture; hypoxic conditions at center of spheroid | No accurate interaction with ECM and cells; standardization difficult | Anticancer drug screening; invasion studies |
| **3D organoids** | Reproduce architecture of *in vivo* tumor accurately | Difficult to produce in large amount for high-throughput screenings | Anticancer drug screening, invasion and extravasation studies |
| **Co-culture on a scaffold** | Complex 3D tissue architecture; complex interaction with TME and ECM and other cells | Poor reproducibility, poor similarity to *in vivo* architecture of tumor | Anticancer drug screening, invasion, and cell infiltration studies |
| **Microfluidic systems** | Able to reproduce fluid flow; constant temperature, chemical gradients and flow pressure which are characteristic of *in vivo* systems | Expensive, non-standardized | Migration/invasion and extravasation studies |

In Figure 4, a schematic representation of the different types of *in vitro* tumor models from (Kristina V. Kitaeva et al., 2020) can be seen.

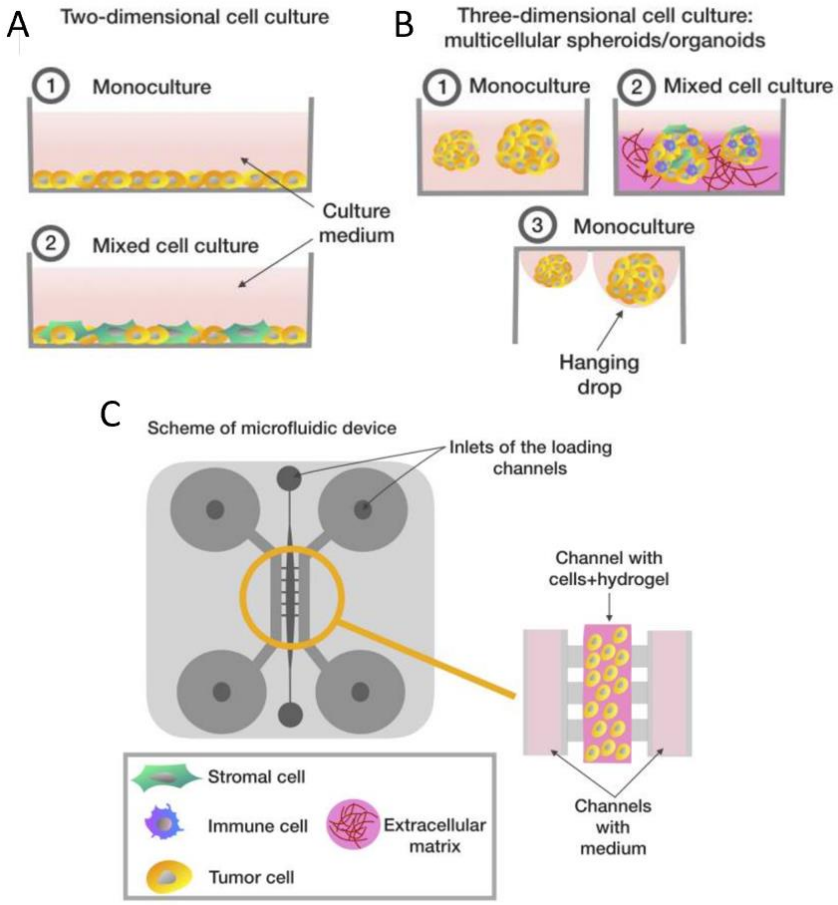


Figure 4 *In vitro* tumor models. (A) 2D monolayer cell culture (1) consisting solely of tumor cells (2) co-culture of tumor and stromal cells (B) 3D tumor models (1) spheroids (2) organoids (3) spheroids made with hanging drop method (C) Example of microfluidic system which is used to determine the invasive potential of tumor cells. Image from (Kristina V. Kitaeva et al., 2020).

### 1.2.1 2D tumor models

*In vivo* mouse models of L1210V leukemia or P388 were used by the National Cancer Institute (NCI) until the 1980s for systematic drug screenings (Kristina V. Kitaeva et al., 2020; Teicher, 2010). These mouse models had high levels of stability and productivity, were convenient when it came to interpretating data, and were relatively cheap. Despite these traits, a notable disadvantage to these mouse models was the inefficiency to identify potential substances for treating solid tumors. This hindrance was at the end of the ‘80s taken into account and an *in vitro* panel for anti-tumor drug screening was established, which consisted of 60 different human tumor cell lines,

termed NCI60 (Kristina V. Kitaeva et al., 2020; Mingaleeva, Solovieva, Blatt, & Rizvanov, 2013)

Testing an anti-tumor drug with the NCI60 panel involves applying a 2D tumor cell culture, grown in a monolayer on a flat surface (Kristina V. Kitaeva et al., 2020; Takimoto, 2003). In the screening's first stage, testing is performed on the three cell lines which are usually the most sensitive to anti-tumor drug therapy: breast adenocarcinoma (MCF7), lung carcinoma (NCI-H460), and glioma (SF-268) (Blatt, Mingaleeva, Khaiboullina, Lombardi, & Rizvanov, 2013; Kristina V. Kitaeva et al., 2020). The pink anionic dye, sulforodamine B, is used to determine the cytotoxicity of the test substance. If the growth of at least one of the cell lines is inhibited by the test substance, testing advances to the next stage which comprises the use of the full NCI60 panel (Kristina V. Kitaeva et al., 2020; Mingaleeva et al., 2013). The screening results of the NCI60 panel was used in 2017 to create the NCI ALMANAC database. This database aided to find new effective combinations of current anti-tumor drugs and launched new clinical trials (Holbeck et al., 2017; Kristina V. Kitaeva et al., 2020)

Similar to the NCI60 panel, in the 1990s the Japanese Foundation for Cancer Research developed a panel out of 30 tumor lines from the NCI60 panel with nine additional tumor cell lines from gastric cancer and breast cancer which are specific to the Japanese population. Hence, 39 cell lines were included in the panel which was accordingly called JCFR39 (Kristina V. Kitaeva et al., 2020; Nakatsu et al., 2007). During clinical trials, however, it became evident that even though some drugs have shown high efficacy in 2D models *in vitro*, they showed low-to-no efficacy in oncology patients (Kristina V. Kitaeva et al., 2020; Shoemaker, 2006). This can partially be explained by the fact that in 2D cultures the cells which are grown do not have a complex 3D tissue architecture and also do not mimic the complex interactions with the TME, ECM or other cells which would exist in the body (Kristina V. Kitaeva et al., 2020; Rizvanov et al., 2010)

### 1.2.2 3D tumor models

As established above, the 2D models do not fully mimic the pathophysiology of tumor cells and the existing level of resistance to chemotherapy or radiotherapy in the *in vivo* tumor niche (L. Chen et al., 2012; Kristina V. Kitaeva et al., 2020). Studies demonstrated that treatment responses and gene expression profiles are more similar to the *in vivo* counterpart when looked at multicellular spheroid 3D models (Kristina V. Kitaeva et al., 2020; Riedl et al., 2017). Liver tumor cells in 3D culture, for example,

have high resistance when treated with drugs, which is similar to the resistance of *in vivo* solid tumors (Kristina V. Kitaeva et al., 2020; Uchida et al., 2010). Hence, breast cancer cell lines when cultured as spheroids, displayed higher resistance to doxorubicin and paclitaxel when compared to 2D culture (Imamura et al., 2015; Kristina V. Kitaeva et al., 2020).

The tumor cells' susceptibility to drugs is significantly changed by the TME. To solve this problem, novel methods were established for cultivating cells utilizing the ECM for modelling spatial organization, as well as adding different types of other cells typically found in the TME to the culture (Kristina V Kitaeva et al., 2019; Kristina V. Kitaeva et al., 2020). 3D co-cultures of fibroblasts and non-small lung cancer cells encapsulated in alginate or embedded in Matrigel are currently used as drug discovery models for analyzing immune cell infiltration (Kristina V. Kitaeva et al., 2020; Osswald, Hedrich, & Sommergruber, 2019). Another high-potential spheroid tumor model for drug screening consists of cancer-associated fibroblasts and pancreatic ductal adenocarcinoma cells which are surrounded by oligomeric type I collagen to create an interstitial ECM support (Kristina V. Kitaeva et al., 2020; Puls et al., 2018).

Apart from spheroids, there is also another promising way to create 3D models of tumor tissue, which is organoids. One of the first described organoids was a mammosphere by Dontu et al. (2003), which allowed the proliferation of mammary stem and progenitor cells into functional acinar/ductal structures (Dontu, Al-Hajj, Abdallah, Clarke, & Wicha, 2003; Kristina V. Kitaeva et al., 2020). In general, two main types of stem cells can be used to receive organoids: organ-restricted, adult stem cells, and pluripotent stem cells, which are embryonic and induced pluripotent stem cells (Clevers, 2016; Kristina V. Kitaeva et al., 2020). Additionally, organoids can also be received by cultivating small tissue fragments and explants on a matrix, or from sorted or cultured cells which can be *in vitro* assembled to organoids (Hu, Todhunter, LaBarge, & Gartner, 2018; Kristina V. Kitaeva et al., 2020). Primary lung cancer tissue organoids displayed high reproduction levels of *in situ* genetic and histological characteristics and have a significant ability to be used in patient-specific drug trials (Kim et al., 2019; Kristina V. Kitaeva et al., 2020). Organoids were also used in studies for modelling pancreatic ductal adenocarcinoma and prostate cancer bone metastasis, both derived from patients (Kristina V. Kitaeva et al., 2020; Lee et al., 2020; Nelson et al., 2020).

### 1.2.3 Microfluidic systems

Microfluidic systems are potential models for reconstructing the microenvironment, microcirculation and migration of cells in tumor tissue. Microfluidic systems are tiny devices which are able to reproduce specific fluid flow, fresh medium, constant temperature, chemical gradients and flow pressure, which are characteristic of *in vivo* systems (Kristina V. Kitaeva et al., 2020; Ruzycka, Cimpan, Rios-Mondragon, & Grudzinski, 2019).

The collagen-Matrigel hydrogel matrix-based microfluidic system made it possible to mimic the microenvironment and experimental conditions to study the invasion and migration of lung adenocarcinoma cells (H1299). Simultaneously, low concentrations of Matrigel facilitated the migration of H1299 cells. However, high concentrations of Matrigel slowed the cell migration, probably due to excessive attachment. It could also be shown that antibody-based integrin blocker usage substantially modulated the cell migration mechanism (Anguiano et al., 2017; Kristina V. Kitaeva et al., 2020). A microfluidic system with persistent nutrient medium supply through a syringe pump has also been described. This system is used to study the matrix metalloproteinase inhibitor effect on forming invadopodia in lung cancer cells, which is distinctive of the cells during invasion (Kristina V. Kitaeva et al., 2020; Wang et al., 2013). Microfluidic systems additionally enable the creation of a model of metastatic tumors, like breast cancer, which allows studying antitumor drug effects on tumor cell migration inhibition (Kristina V. Kitaeva et al., 2020; Mi et al., 2016). To mimic the extravasation process, a microfluidic system was established with two microfluidic channels and a porous membrane in-between. The first microchannel serves as the equivalent to the vascular system and contains isolated primary endothelial cells from the pulmonary artery. The second microchannel functions as a reservoir to collect tumor cells which are migrating. Under these circumstances, the endothelial cells display an *in vivo*-like behavior under flow conditions. The green fluorescent protein (GFP)-labelled tumor cells of mesenchymal or epithelial origin could be detected via vital imaging, which displayed tight attachment of tumor cells to the endothelial membrane (Kristina V. Kitaeva et al., 2020; Kühlbach, Da Luz, Baganz, Hass, & Mueller, 2018)

## 1.3 3D bioprinting

3D bioprinting is a highly studied method for many aspects of tissue engineering as it offers effective control over cell distribution and scaffold fabrication (Daly et al., 2016; Kesti et al., 2015). In modern 3D-bioprinting techniques, the printing resolution reaches a value of 10 to 1000µm, which is a rather wide range and shows the flexibility of bioprinting compared to other methods of assembly like porous or molding scaffolds (Daly et al., 2016; Kesti et al., 2015).

Based on the deposition of biomaterials, 3D bioprinting is an additive manufacturing technique. Therefore, it can form tissue-like structures in micrometer scale with either encapsulated cells or cells added later on (Derakhshanfar et al., 2018). Often, the movements of extruders which eject the bioink are controlled by a three-axis mechanical platform in the required shape and algorithm (Derakhshanfar et al., 2018). The movement of the platform is guided by coordinates which are established by the designer and saved in a file format which can be easily followed by the printer (Derakhshanfar et al., 2018). Recently, the development and application of 3D bioprinting has risen constantly, mostly due to simplicity, cost-effectiveness, precise deposition and controllability of cell distribution (Bishop et al., 2017; Derakhshanfar et al., 2018).

The following table (Table 2) is a short summary of bioprinting studies, mainly with extrusion bioprinting as method of bioprinting, but showing the versatility of 3D bioprinting in research, and also the diversity of bioinks, which will be thematized later.

Table 2. Short summary of bioprinting studies in recent years (Derakhshanfar et al., 2018).

| **Method** | **Material** | **Application** | **Short research summary** | **Ref** |
|---|---|---|---|---|
| **Extrusion** | Nanocellulose | Wound dressing | Development of 3D porous structures | (Rees et al., 2015) |
| **Extrusion** | Alginate | Bioprinting of tissue/organ | New micro-fabrication method for creation of tissue strands | (Yu & Ozbolat, 2014) |
| **Extrusion** | Collagen/gelatin/ alginate hydrogel | Tissue engineering in general | Cell-laden hydrogel for proliferation studies | (Z. Wu et al., 2016) |
| **Droplet-based** | Polyethylene glycol | Soft-tissue model | Integrative bioprinting | (Rimann, Bono, Annaheim, Bleisch, & Graf-Hausner, 2016) |
| **Extrusion** | Hyaluronic acid and gelatin | Liver constructs | Development of a bioink | (Skardal et al., 2015) |
| **Extrusion** | Spider silk protein, human fibroblasts | Tissue engineering in general | Development of novel bioink | (Schacht et al., 2015) |

Before heading into the various 3D-bioprinting methods which are available and explaining how they work, a short table explaining the advantages, disadvantages and many more is shown in Table 3.

Table 3: Overview of bioprinting methods in use (Derakhshanfar et al., 2018).

| | **Extrusion** | **Inkjet** | **Stereo-lithography** | **Laser-assisted** | **Direct light bioprinting** |
|---|---|---|---|---|---|
| **Pros** | Simple, various biomaterials possible as bioink, high cell densities possible | Low viscosity biomaterials possible, fast, low cost, high resolution | Nozzle-free, fast, high accuracy and cell viability | Biomaterials in solid and liquid phases possible, high resolution | Fast, high resolution, nozzle free, |
| **Cons** | Only viscous liquids | No continuous flow possible, poor vertical structures, low cell density | UV light source → toxicity to cells, lack of printing multiple cell types | Thermal damage to cells, high cost | Lack of printing multiple cell types |
| **Speed** | Slow | Fast | Fast | Medium | Fast |
| **Cost** | Moderate | Low | Low | High | Low |
| **Vertical printing ability** | Good | Poor | Good | Medium | Good |
| **Cell viability** | <90% | 80–95% | >90% | <85% | >90% |
| **Resolution** | 100µm | 50µm | 100µm | 10µm | 50µm |

| | | | | | |
|---|---|---|---|---|---|
| **Ref** | (Billiet, Vandenhaute, Schelfhout, Van Vlierberghe, & Dubruel, 2012; Dai et al., 2017; Holzl et al.; Ozbolat & Yu, 2013; Xu, Baicu, Aho, Zile, & Boland, 2009; Zongjie, Abdulla, & Parker, 2015) | (Billiet et al., 2012; Gao, Yonezawa, Hubbell, Dai, & Cui, 2015; Holzl et al.; Murphy & Atala, 2014; Ozbolat & Yu, 2013; Saunders & Derby, 2014; Xu et al., 2009) | (Billiet et al., 2012; de Gruijl, van Kranen, & Mullenders, 2001; Gauvin et al., 2012; He et al., 2016; Ozbolat & Yu, 2013; K. M. Park, Lewis, & Gerecht, 2017; Sinha & Häder, 2002; Xu et al., 2009; Zongjie et al., 2015) | (Billiet et al., 2012; Murphy & Atala, 2014; Ozbolat & Yu, 2013; Xu et al., 2009; Zongjie et al., 2015) | (Bernal et al., 2019; Derakhshanfar et al., 2018; Lim et al., 2018; Petta et al., 2018; Zheng et al., 2020) |

### 1.3.1 Extrusion

Extrusion-based bioprinting—as the name suggests—extrudes a biomaterial, also referred to as bioink, through a nozzle either pneumatically or mechanically (Z. Gu, Fu, Lin, & He, 2020). This forms continuous micro filaments which are deposited in a layer-by-layer fashion, to finally create the desired structure (Z. Gu et al., 2020). The bioink is printed onto a substrate which can either be solid, such as a culture dish, or liquid, like growth medium (Z. Gu et al., 2020). The shape and architecture of the bioprinted structure can be defined by a 3D computer model, which then is translated into the path the nozzle will be going (You, Eames, & Chen, 2017). The final bioprinted structure is influenced by a variety of factors, like temperature, extrusion pressure, nozzle diameter, movement and extrusion speed, etc. (Z. Gu et al., 2020). Three often used actuation modes of dispensing liquid can be used: piston, pneumatic and screw driven. The different modes are shown in Figure 5.

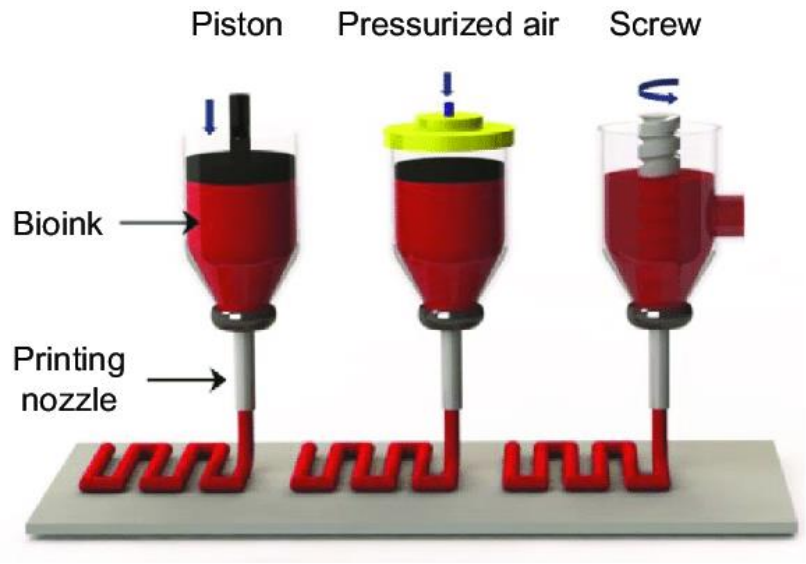


Figure 5. Different extrusion bioprinting techniques. Piston- driven (left). Pneumatic-driven (middle). Screw-driven (right). Image from (Pereira & Bártolo, 2015).

Pneumatic-driven extrusion bioprinting uses compressed air to dispense the bioink from a syringe and nozzle at a controllable flow rate (Z. Gu et al., 2020). The accuracy of deposition is dependent on the bioink's flow properties and can be affected by viscosity (Chen, X. B., Schoenau, , & Zhang 2002; Ning & Chen, 2017). The mechanically driven extrusion methods, piston and screw, push the bioink by a linear moving piston or a rotating screw (Ning & Chen, 2017; Valkenaers, Vogeler, Voet, & Kruth, 2013). Both are known to be able to provide great deposition forces, thus are of benefit for printing high viscosity bioinks (Ning & Chen, 2017). However, this large driving force can be of disadvantage as it may induce cell membrane rupture and these mechanically driven mechanisms usually require complex components (X. B. Chen, 2006; Ning & Chen, 2017).

### 1.3.2 Inkjet

At the end of the 19$^{th}$ century Lord Rayleigh studied the instability of jets and how these jets break into drops (X. Li et al., 2020; Rayleigh, 1878, 1891). His work was the base for the inkjet technologies we have today. Due to this theory, continuous inkjet printing was established which was able to produce controllable high-speed droplet flow (X. Li et al., 2020; Schneider & Hendricks, 1964; Sweet, 1965). Soon thereafter, inkjet devices were invented with drop-on-demand technology which allowed to eject a droplet only after a digital signal was received (X. Li et al., 2020). This was then developed further and gave us the inkjet printers from big companies like HP and Canon which we know today.

In recent years, many life science researchers have realized that the drop-on-demand and noncontact traits of inkjet printing might help with accurately patterning biomaterials without waste and contamination (X. Li et al., 2020).

However, 3D inkjet bioprinting inkjet application has been limited when compared to the extrusion counterpart, although the first bioprinting studies were actually based on inkjet, in 2006 by Thomas Boland et. al. The major reason is its inherent inability to provide continuous flow (Derakhshanfar et al., 2018; Ozbolat & Yu, 2013). Bioinks which are printable via inkjet printing should have viscosities of lower than 10 mPa*s. When compared to other methods, inkjet offers fast speeds in fabrication, but low cell densities (Derakhshanfar et al., 2018; Holzl et al.). Inkjet printing methods can in general be classified into three main groups: continuous-inkjet, electro-hydrodynamic jet, and drop-on-demand inkjet bioprinting. The latter—which happens to be the most common and largest category—consists out of three sub-categories: thermal, piezoelectric and electrostatic (Derakhshanfar et al., 2018; Gudapati, Dey, & Ozbolat, 2016). All Inkjet methods can be seen in the figure below.

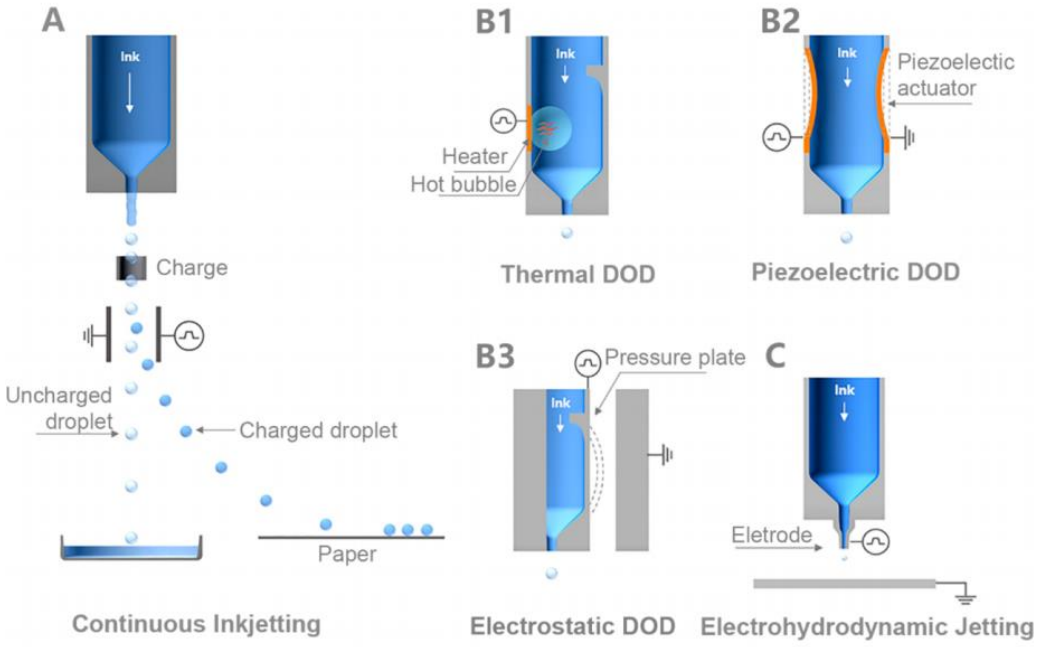


Figure 6. Schematic representation of inkjet bioprinting methods. (A) Continuous inkjet. The liquid is ejected to form continuous droplets, the designation of each droplet is controlled by giving the droplets a charge and applying an electric field. (B) Drop-on-demand (DOD) inkjet bioprinting. (B1) Thermal DOD, ejects droplets via generating bubbles through heat. (B2) Piezoelectric DOD, produces droplets via a piezoelectric actuator, which deforms the bioink chamber. (B3) Electrostatic DOD, ejects droplets via deformation of a pressure plate. (C) Electrodynamic Inkjet bioprinting generates droplets via a high voltage electric field. Image from (X. Li et al., 2020)

Continuous inkjet printing refers to the method where the ink flows out of a nozzle with controlled pressure, which then splits into individual droplets. Afterwards, these droplets are charged by passing through charging plates. The charged droplets pass through deflection plates, controlling the droplet placement with adjustment of the field strength applied (Iwanaga, Saito, Sanae, & Nakamura, 2013; X. Li et al., 2020; Sweet, 1965). Non-charged droplets are not used and are usually recovered to minimize waste, which might lead to unavoidable contamination. This contamination issue, as well as the complexity of the device, makes it less suitable in laboratory use for bioprinting, which is why they are not used for bioprinting yet (X. Li et al., 2020). This method's schematic representation is shown in Figure 6A.

The second option for inkjet bioprinting is electrohydrodynamic inkjet bioprinting. This method uses an electric field that pulls the droplets through the orifice of a nozzle (Donderwinkel, van Hest, & Cameron, 2017). The advantage of this method is the ability to utilize highly concentrated bioinks and small orifice diameters (Donderwinkel et al., 2017; Gudapati et al., 2016). However, due to the application of high pressure on the droplets and tiny orifice diameters, large shear forces are produced and therefore cells can be damaged (Donderwinkel et al., 2017; Gudapati et al., 2016). This method's schematic representation is shown in Figure 6B.

As mentioned above, the last option for inkjet bioprinting, drop-on-demand (DOD), can be further divided into three subsections. Thermal, piezoelectric, and electrostatic. Thermal DOD bioprinting generates small air bubbles via heating within the printhead, the collapsing of these air bubbles causes a pressure pulse which in turn is responsible for ejecting ink drops out of the nozzle in diverse volumes ranging from 10 to 150pL (X. Cui, Boland, D'Lima, & Lotz, 2012). The size of the droplets depends on the applied temperature gradient, current pulse frequency and viscosity of the ink used (X. Cui et al., 2012). A schematic of thermal DOD bioprinting can be seen in Figure 6B1. Thermal DOD, is not as frequently used due to the heat which has to be employed (Derakhshanfar et al., 2018). In piezoelectric DOD bioprinting, a pulse is created via deformation of the bioink chamber by the piezoelectric actuator (Derby, 2008). This deformation suddenly changes the volume within the chamber and causes a pressure wave, thus the surface tension at the orifice of the nozzle is overcome, ejecting a droplet of bioink (Gudapati et al., 2016; Singh, Haverinen, Dhagat, & Jabbour, 2010). A schematic of piezoelectric DOD bioprinting can be seen in Figure 6B2. The last technique, electrostatic DOD bioprinting, generates droplets by briefly increasing the ink chamber's volume, but—unlike the thermal method—without heating (Gudapati et

al., 2016; Kamisuki et al., 1998). This temporary increase in volume is achieved by means of a pressure plate, which deflects when a pulse of voltage is applied between an electrode and the plate itself (Gudapati et al., 2016; Nishiyama et al., 2009). The pressure plate recovers to its native shape in absence of the pulse, which is when the droplet ejects (Gudapati et al., 2016). A schematic of electrostatic DOD bioprinting can be seen in Figure 6B3.

### 1.3.3 Laser-assisted bioprinting

Laser-assisted bioprinting (LAB) deposits bioinks onto a substrate with a laser as the energy source (J. Li, Chen, Fan, & Zhou, 2016). This method mostly consists out of three main parts: a pulsed laser source, a liquid bioink coated ribbon, and a receiving substrate (Jana & Lerman, 2015; J. Li et al., 2016). The pulsed laser irradiates the coated ribbon. This causes the bioink on the ribbon to evaporate, building a vapor pocket. The bioink reaches the receiving substrate as droplets (J. Li et al., 2016). The substrate receiving the bioink is typically made out of a cell culture medium or biopolymer, to maintain cellular adhesion and promote cell growth after cell transfer from the ribbon (J. Li et al., 2016). Nanosecond lasers with UV or around-UV wavelengths are mainly used as energy sources for printing hydrogels, proteins and cells (Catros et al., 2011; J. Li et al., 2016). The resolution which can be achieved with LAB varies from pico- to micro-scale, and is affected by a variety of factors: the thickness of the bioink used, the rheological properties of the bioink, the energy of the laser pulse, the printing speed, and the structure organization (Guillemot, Souquet, Catros, & Guillotin, 2010; Guillemot, Souquet, Catros, Guillotin, et al., 2010; J. Li et al., 2016). A schematic representation of LAB can be seen in Figure 7.

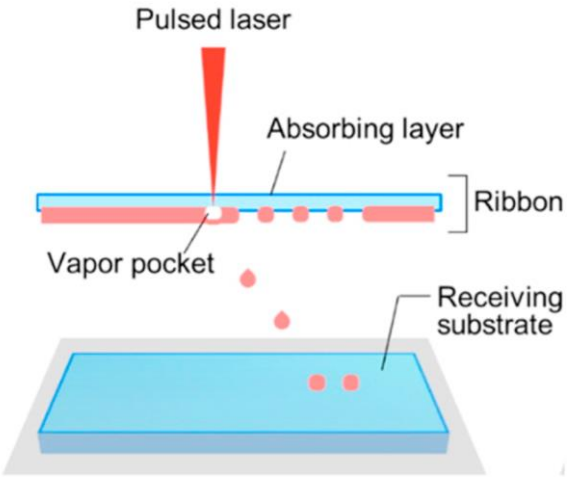


Figure 7. Schematic representation of Laser-assisted bioprinting. Image from (Jang, 2017).

### 1.3.4 Stereolithography

Stereolithography (SLA) 3D bioprinting has developed to be a popular bioprinting method which addresses the requirements of tissue scaffold fabrication (Kumar & Kim, 2020). The method first appeared in the 1980s and is therefore to be considered the oldest approach for bioprinting which facilitates the generation of complex 3D structures with high precision and resolution (Iram, Riaz, & Iqbal, 2019; J. H. Park, Jang, Lee, & Cho, 2017). In this method, a single beam laser is used for crosslinking or polymerizing a photopolymer (Iram et al., 2019; G.-H. Wu & Hsu, 2015). The irradiation of the laser beam is spatially controlled to layer the bioink by selective photopolymerization, generating a 2D pattern (H. Cui, Nowicki, Fisher, & Zhang, 2017; Iram et al., 2019). The SLA bioprinting method creates a 3D structure by continuously layering the created 2D patterns on top of each other (H. Cui et al., 2017; Iram et al., 2019). The photopolymerization induction in this technique is attained either by single-photon or two-photon absorptions. It is mainly controlled by factors including irradiation time, light intensity and concentration of the photoinitiator (Billiet et al., 2012; H. Cui et al., 2017; Iram et al., 2019). Conventional SLA-based bioprinting can be further divided into two categories: beam-scanning and mask-image-projections (H. Cui et al., 2017; Iram et al., 2019; Zorlutuna et al., 2012).

In the beam-scanning technique, the 2D patterns are drawn and solidified through the use of a focused laser beam (Figure 8) (Iram et al., 2019; J. H. Park et al., 2017). Factors which influence the resolution include power, wavelength, exposure velocity and time, laser spot size and absorption, and scattering (H. Cui et al., 2017; Iram et al., 2019; Miao et al., 2016; W. Zhu et al., 2015).

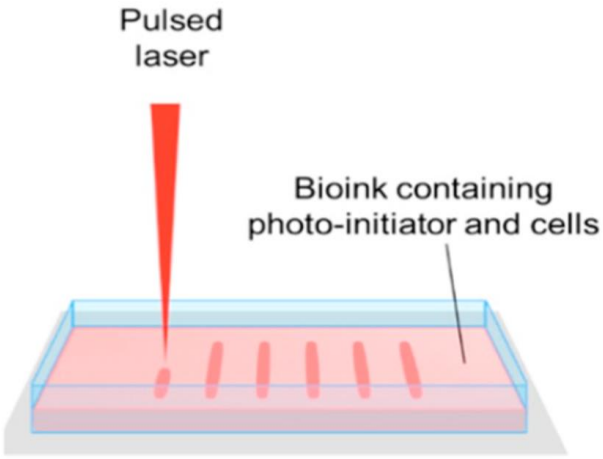


Figure 8. Schematic representation of beam-scanning SLA bioprinting. Image from (Jang, 2017).

The technique used in this project is a mask-image-projection process which uses digital light processing (DLP) to generate a defined mask image (B. K. Gu et al., 2016; Iram et al., 2019; Skoog, Goering, & Narayan, 2014; Stansbury & Idacavage, 2016). The DLP system uses a device to generate an image like the digital micro mirror, which efficiently solidifies one entire 2D layer with a single projection, a schematic representation of which can be seen in Figure 9 (Iram et al., 2019; J. H. Park et al., 2017). This consequently results in generating a 2D image pattern within a short period of time (Iram et al., 2019; J. H. Park et al., 2017). Hence, when compared to the beam-scanning technique, mask-image-projection printing is a rapid technique (Iram et al., 2019).

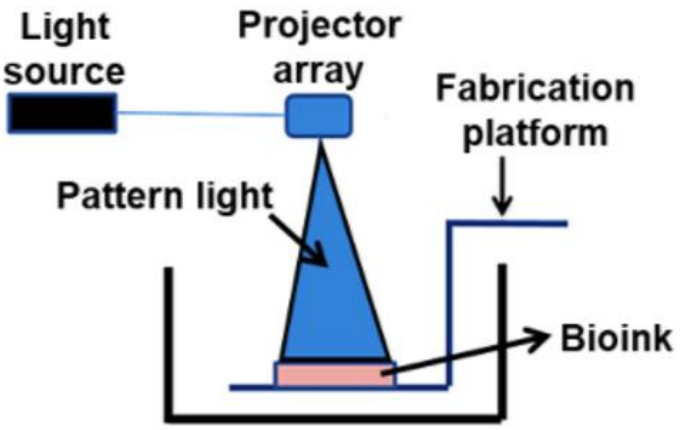


Figure 9. Schematic representation of mask-image-projection SLA bioprinting. Image from (Loai et al., 2019).

However, the limitation of both SLA bioprinting methods is the scarcity of suitable bioinks to use (Raman & Bashir, 2015).

### 1.3.5 Bioink

Amid all the research on bioinks, there are some which stand out specifically by the benefits they are offering. New methods, spectacular properties and specific applications are some of the main reasons making the studies regarding bioink inspiring (Derakhshanfar et al., 2018; Poologasundarampillai & Nommeots-Nomm, 2017).

There are many possibilities for materials in bioprinting, here are some of the most used: polymers, hydrogels, ceramics, and composite. Polymers are among the most commonly used bioinks (Mobaraki, Ghaffari, Yazdanpanah, Luo, & Mills, 2020). They are mainly used due to their biocompatibility, low cost, secure processing and

degradation (Mobaraki et al., 2020). Another advantage of polymer as bioink is its ability to change its form (Mobaraki et al., 2020).

Water-soluble polymers, also known as hydrogels, are also a commonly used ink for bioprinting, due to their promising environments for cell growth and chemical configuration (Lei & Wang, 2016; Mobaraki et al., 2020). Hydrogels consist of 3D polymeric networks which can hold much water. Consequently, they are known to be materials which are biocompatible and provide a low-polymer, high-water content environment which is more cell-friendly (Di Bella, Fosang, Donati, Wallace, & Choong, 2015; Mobaraki et al., 2020; Raza et al., 2018). Lately, hydrogels have seen significant usage in a wide array of biomedical applications, including biosensors, wound dressings, cell encapsulations, and also 3D bioprinting (Kesti et al., 2015; Mobaraki et al., 2020). Especially in tissue engineering, the fabrication of hydrogel scaffolds is a key component in a variety of applications, due to their permeability to nutrients, oxygen, and other water-soluble compounds (Mobaraki et al., 2020; Thomas, Craig Fryman, Liu, & Mason, 2009). In general, there are three types of hydrogels which are commonly used in tissue engineering applications: synthetic, natural and blends of synthetic and natural (Buwalda et al., 2014; Mobaraki et al., 2020). Mixing a precursor solution with a cell suspension and subsequent polymerization or crosslinking of the mixture causes the cells to be encapsulated within the hydrogel. This can be done with various cell types as well as tissue spheroids and at least one hydrogel forming polymer. Due to their potential to be formulated for all bioprinting methods mentioned above, cell-laden hydrogels are widely used bioinks.

Natural polymers have short, repeating units with directional and reversible non-covalent bonding interactions—like hydrogen bonding, π- π, and metal coordination (Brunsveld, Folmer, Meijer, & Sijbesma, 2001; Mobaraki et al., 2020). The non-covalent bonds are under high stress and can be reversibly broken to dissipate energy. The reversibility of these bonds, is also a key factor that leads to its shear-thinning properties which facilitate their usage in bioprinting (Chimene, Lennox, Kaunas, & Gaharwar, 2016; Mobaraki et al., 2020). The essential natural polymers which are utilized in many 3D bioprinting applications are collagen, fibrin, alginate, silk, chitosan, hyaluronic acid, gelatin and gelatin methacryloyl (GelMA) (Kolesky et al., 2014; Malda et al., 2013; Mobaraki et al., 2020).

#### 1.3.5.1 GelMA

Ever since gelatin methacryloyl (GelMA) was first described by Van Den Bulcke et al., it has established a reputation to be one of the most versatile available hydrogels for 3D bioprinting and 3D cell culture (Klotz, Gawlitta, Rosenberg, Malda, & Melchels, 2016; Pepelanova, Kruppa, Scheper, & Lavrentieva, 2018; Van Den Bulcke et al., 2000). GelMA is a semi-synthetic hydrogel, that enables the exploitation of the gelatin molecule's biological signals, while allowing mechanical property control (Pepelanova et al., 2018; Ruedinger, Lavrentieva, Blume, Pepelanova, & Scheper, 2015). The hydrogel is synthesized by gelatin derivatization with methacrylic anhydride, resulting in the lysine and hydroxyl residue's modification with methacrylate and methacrylamide side groups, as can be seen in Figure 10 (Pepelanova et al., 2018; Yue et al., 2015). Even after derivatization, gelatin retains many of its attractive attributes as a biomaterial. It still shows thermoreversible physical gelation, and maintains its biological promoting properties, established on metalloprotease digestion sites and integrin-binding sequences (Pepelanova et al., 2018). The GelMA hydrogel can therefore provide the cells with an aqueous environment and supports their proliferation, growth, and adhesion (Pepelanova et al., 2018). Compared to gelatin, however, the methacryloyl side group modification allows GelMA to undergo quick polymerization in the presence of a photoinitiator and UV light, resulting in a covalent link through the generation of a methacryloyl backbone (Pepelanova et al., 2018; Yue et al., 2015). This trait gives GelMA stability at physiological temperature and grants mechanical property fine-tuning. Furthermore, the final material is transparent, which facilitates analysis with a microscope (Pepelanova et al., 2018).

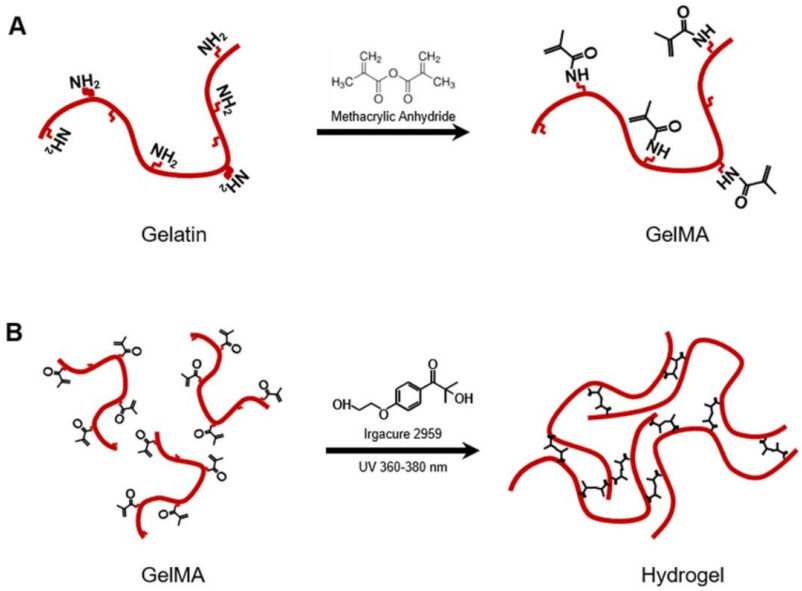


Figure 10. Synthesis of gelatin methacryloyl (GelMA). (A) Gelatin is mixed with methacrylic anhydride (MA) to introduce a methacryloyl group to the reactive hydroxyl and amine groups of the amino acid residues. (B) Photocrosslinking of GelMA with UV irradiation to form a hydrogel matrix. The free radicals originating from the photoiniatiator initiate a chain polymerization with the methacryloyl substitution. Image from (Yoon et al., 2016).

GelMA is thus renowned for its superior degradability, biocompatibility and low cost (Catoira, Fusaro, Di Francesco, Ramella, & Boccafoschi, 2019). Due to these qualities, GelMA has been extensively used for 3D cell culture applications and as a tool for tissue engineering (Loessner et al., 2016; Pepelanova et al., 2018).

## 1.4 Aim of the project

This master thesis project was conducted with two main goals in mind. The first aim was to establish a 3D cholangiocarcinoma-on-a-chip and triculture system with functional microchannels consisting of GelMA. This cholangiocarcinoma-on-a-chip model was evaluated as an effective cytotoxic drug-testing platform. Also, a comparison with 2D tumor cell culture system was performed to show which more accurately depicts the *in vivo* counterpart. This was on the one hand done via RNA-sequencing (RNA-seq) and on the other hand via cell sensitization to cyclophosphamide.

The second aim of the master thesis project was to design and fabricate this tumor-on-a-chip model via bioprinting methods. Therefore, a model was printed with a digital micromirror device (DMD) based 3D bioprinting platform and GelMA as bioink. Additionally, these models incorporated three cell types within the GelMA construct which mimics the microstructure, present *in vivo.* These three cell types, which are essential for the cholangiocarcinoma microenvironment, are RBE (cholangiocarcinoma cell line), Hep-G2 (liver cancer cell line), and HUVEC (human umbilical vein endothelial cell).

# 2. METHODS

## 2.1 GelMA synthesis

Based on previously published procedures, batches of GelMA were synthesized (Yue et al., 2015; M. Zhu et al., 2019). A 10% (wt./vol) gelatin powder (Sigma-Aldrich, St. Louis, MO, USA) solution was prepared at 50°C in 100mL phosphate buffered saline (PBS; CB, pH=10) buffer with a ring velocity of 240 to 300 rounds per minute (rpm) until completely dissolved. With a pipette tip Methacrylic anhydride (MAA, Sigma-Aldrich, St. Louis, MO, USA) was added in a dropwise fashion. To ensure a homogenous mixture, the stir velocity was increased to 400 rpm. For a methacrylation degree of around 90–100% (High grade GelMA), 1mL of MAA was dripped into the solution. For a methacrylation degree of about 55–65% (Medium grade GelMA), only 400µL were added. Afterwards, the solution was mixed for 1.5h at 300rpm and 50°C. Then the solution was diluted 1:2 with warm buffer and left stirring for another 20 minutes (min). Following the dilution, the solution was dialyzed against distilled water at 40°C with membrane tubing (Spectro/Por molecularporous membrane tubing, MWCO 12–14.000, Fisher Scientific); to remove unreacted MA, the water was swapped out twice a day for one week. Then the GelMA was filtered through a 0.22µm vacuum filter, put into 50mL conical plastic tubes, frozen overnight at -80°C, and lyophilized for five days. The freeze-dried GelMA was wrapped with aluminum foil and kept at 4°C until further use.

## 2.2 Cell Culture

The cholangiocarcinoma cells (RBEs) were maintained in RPMI 1640 (Gibco, Invitrogen) with addition of 10% fetal bovine serum (FBS; Gibco, Invitrogen). HepG2 cells were cultured in DMEM (Gibco, Invitrogen), also with 10% FBS. HUVEC cells were maintained in endothelial cell medium. 1% penicillin and streptomycin were added to all cultured cells. Cells were incubated at 37°C and 5% $CO_2$. Medium changes were performed as necessary.

## 2.3 Fabrication of GelMA-based functional microchannel

GelMA constructs with functional microchannels were fabricated by using a poly(methacrylic acid) (PMMA) mold. Four pieces were fabricated via laser cutting. Two of these pieces had two, four or six matching holes (diameter of 0.5–0.6mm) on them, for holding 23G needles. All four pieces were assembled into a rectangle in a fashion that the two pieces with holes where facing each other. The chamber had a volume of 344µL and its internal dimensions (width/depth/height) were 8mm, 10mm, and 4.3mm

respectively. The chamber and needles were then sterilized by placing them in 70% Ethanol overnight (o/n) and afterwards placed under UV light for 30min. The tools needed to assemble the chamber were autoclaved with saturated steam at 106kPa and 121–132°C.

The next step was to create the cell embedded 3D structure with integrated cylindrical microchannels. Therefore, a solution was prepared with the previously synthesized GelMA (5% wt./vol.), LAP photoinitiator (0.2% wt./vol.) and Dulbecco's phosphate-buffered saline (DPBS; Gibco). The mixture was left to dissolve at 37°C and afterwards filtered with syringe filters (Target2$^{TM}$ PTFE Syringe filters, 0.2µm pore size). The needles were placed into the mold, going through two holes on opposite sites. The mold was filled with the prepared GelMA solution and placed under UV light for 40 seconds (Omnicure S2000, Excelitas, Waltham, MA, USA) for crosslinking; so that the GelMA hardens. Subsequently, the needles were removed, and the mold was disassembled. Hollow duct-like microchannels were left where the needles resided in the GelMA. The construct was transferred to a petri dish with FBS (100%) for about 30min; to improve cell adhesion. Into every other microchannel RBE-enhanced green fluorescent protein (EGFP) cell suspension (1x10^7 cells/mL) was injected and incubated at 37°C and 5% $CO_2$. The constructs were rotated every 30min over the course of the following three hours to improve adhesion uniformity. After the cells attached to the microchannel's inner surface, the microchannels were flushed gently with media to remove the remaining non-adherent cells. After 24h, the remaining channels were seeded with HUVEC-red fluorescent protein (RFP) cells. Lastly, the constructs were transferred into a larger Hep-G2-cell-containing GelMA construct and crosslinked together for further co-culture.

## 2.4 Fluorescence imaging to validate the co-culture system

CellTrace Blue (ThermoFisher, MA, USA) was added to the Hep-G2 culture, before seeding the co-culture chip. For visualization of HUVEC and RBE cells, pCMV-LifeAct-RFP (Ibidi) was applied to the fluorescence-tag LifeAct, an actin-binding amino acid. In the following, the overexpressed lentiviral vectors for LifeAct-EGFP and LifeAct-RFP, which are pH5674-LifeAct-RFP/EGFP, were constructed. RBE-LifeAct-EGFP and HUVEC-LifeAct-RFP were then retrieved by lenti-LifeAct-EGFP or lenti-LifeAct-RFP conducted transgenesis of RBE or HUVESs, respectively, for the microchannel visualization.

## 2.5 Compressive modulus

The compressive modulus of GelMA constructs was tested with a low force universal testing system (Instron). The samples were left in their dimensions of 10mm, 8mm, and 4.3mm. Before measuring, the zero gap was defined via the system's software. The measurements were performed at 1% L0 /s (0.4mm/s). After loading each sample, for cyclic tests, five sequential cycles from 0% to 10% were performed. The process was repeated to ensure reproducibility of the results up until 10% strain. The following five cycles were carried out with a strain of 0% to 20%. The final round of cycles was done with rising strain, starting at a strain of 0% and returning to 0% after each threshold reached: 10%; 20%; 30%; 40%.

## 2.6 Immunostaining assay

The microchannels were immunostained with anti-human CD31 antibody with Alexa 594-conjugated secondary antibody (goat anti-mouse IgG) and Alexa 488 anti-human epidermal growth factor receptor (EGFR) antibody, respectively. The constructs were washed with PBS thrice, fixed with 4% para formaldehyde (PFA) in PBS at 37°C for 15min. Followed by washing thrice with PBS at room temperature, and permeation with 0.1% Triton X-100 at 37°C for 20min. The samples were subsequently blocked with 5% bovine serum albumin (BSA) at room temperature for 30min, followed by an overnight incubation with primary CD31 antibody or Alexa 488 anti-human EGFR antibody at 4°C. Again, it was washed with PBS three times. To visualize CD31 the sample was incubated for 2h with secondary antibody in 5% BSA. After staining, the samples were imaged at room temperature.

## 2.7 RNA-sequencing assays

To get a better understanding about the genes being expressed by the cells within the construct, they were sent for RNA sequencing. The chips were, with the same procedure as before, carefully fabricated. The exception to before being that HUVECs and RBEs were injected instead of their transfected counterparts, HUVEC-RFPs and RBE-EGFPs. The cells were allowed to grow for a week, for fully surrounding the channels. Special attention was taken with the constructs, in regard to contact with other organisms, to exclude RNA contamination. Chips were stored at -20°C and sent for sequencing (BGI).

## 2.8 Establishment of DMD based 3D bioprinting platform

3D-structures were printed with a digital light processing (DLP) bioprinter which was made in the laboratory. The printer consists out of a 450nm electronic laser, 3 optical lenses (f=10cm; f=7.5cm and f=5cm), a DMD (TI DLP LightCrafter 6500 Evaluation Module) to adjust focus, a 10cm leadscrew with shaft coupler, a stepper motor and its driver (Easydriver, 1/8 microstepping configuration), an Aruino Mega board to control the system and two limit switch sensors.

The building plate, upon which the structure was printed on, was attached to the lead screw with screws and laser-cut acrylic pieces. At the same time, the lead screw was connected to the stepper motor's shaft via the coupler. The lead screw was needed to convert rotational motion into linear displacement, resulting in up and down movement of the building platform, depending on the spin direction of the motor. The motor was controlled via the Arduino Mega board (ARMega 2560) and the driver (Easydriver v2). The Arduino was linked to a computer with the software controlling the projected images and telling the Arduino when and in which direction to move the motor. A vat with a transparent ultra-thin polydimethylsiloxane (PDMS) bottom was custom made, to fit the bioprinter set-up. The stage where the vat resides was built with metallic and acrylic rods.

The first step for printing was to fill up three quarters of the vat with the bioink and place the vat into the right position. Afterwards, the building plate was submerged into the bioink so that 100µm of bioink were on top of the building plate. Subsequently, the pattern was projected onto the surface of the bioink, crosslinking the first layer in the pattern of the projected image. Then the building plate was moved down to the desired layer thickness. The procedure was repeated in a layer-by-layer fashion. Every time the building plate moved down, new liquid bioink flowed above and could be crosslinked on top, which also attached to the layer before. To define the projected patterns, a 3D computer model (STL) was broken down into 2D images and given to the software controlling the printing. For this, Form Labs open source slicer (https://formlabs.com/blog/open-source-dlp-slicer/) was used. The control and projection software were developed by the lab specifically for the bioprinter.

## 2.9 Design and fabrication of DMD-bioprinted chips

The bioink was prepared by mixing a solution of 20% GelMA with sodium persulfate (SPS) and ruthenium (RU) at 40 and 4mM, respectively. This solution was diluted 1:1 with DPBS leading to a final concentration of 10% GelMA, 20mM SPS and 2mM RU.

5µL of photo absorber were added. The mixture was then placed in the vat, for later printing. Incorporation of cells into the ink, was done by substituting DPBS in the diluting step with cell suspension (1x10^7 cells/ml in medium).

Lastly, after printing of the construct was finished, the construct was transferred from the building plate into DPBS to wash out the remaining ink. The printing process was performed in a dark room with as little light as possible, due to the ink's photosensitivity.

## 2.10 Cell viability assay

The cultured cells in the GelMA constructs were tested for viability. Therefore, a live/dead assay (LIVE/DEAD Viability/ Cytotoxocity Kit, for mammalian cells, by ThermoFisher) was performed on the cell seeded chips. Calcein-AM (2mM stock) and ethidium homodimer-1 (EthD-1, 2mM stock) solutions were prepared under the flow hood, while the lights were kept off and wrapping the tubes in aluminum foil, to protect them from light. Calcein-AM was diluted 1:1000 with DPBS for a final concentration of 2µM. EthD-1 was diluted 1:500 with DPBS for a final concentration of 4µM. Both were stored at 4°C before use and kept wrapped in aluminum foil. After preparing the solutions, the samples were taken from the incubator and washed three times with DPBS. Then the samples were covered with staining solution and put into the incubator (37°C/ 5% $CO_2$) for 25min. Afterwards, the samples were washed with DPBS twice. The samples were observed under the fluorescent microscope with 488nm and 594nm excitations for taking pictures. The assay was performed on day one, three, five, seven, and nine, after seeding cells.

## 2.11 Image acquisition and processing

The images were acquired with the help of two different microscopes. Brightfield and immunofluorescent images were taken with a fluorescence microscope (Eclipse, Nikon, Japan). Confocal images were obtained with a Zeiss Confocal Microscope (LSM880, with Airyscan, Carl Zeiss, Germany). The fluorescence microscope with a set of wavelengths of 510nm and 588nm was used to visualize RBE-EGFP and HUVEC-RFP, respectively. The same microscope with wavelengths of 488nm and 594nm was used on cell viability assay samples. Pictures were taken and saved as tiff format. ImageJ was utilized for analyzing and processing images. Using ImageJ, different channels were merged, 3D reconstruction was rendered for confocal images and stacks, scale bars were added, and brightness and contrast were adjusted.

# 3. RESULTS

## 3.1 GelMA-based 3D functional microchannels

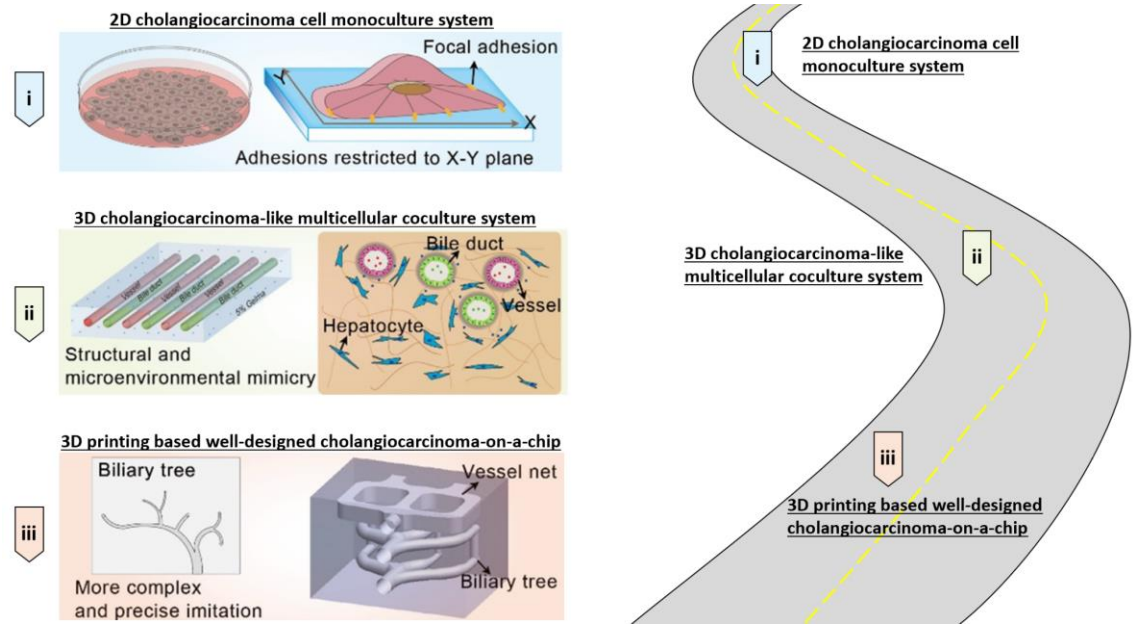


Figure 11: Project Overview - Cholangiocarcinoma model's progress. (i) 2D cholangiocarcinoma cell culture has limitations with focal adhesion of cells and unfaithful representation of tissue (ii) Simple 3D co-culture system. Higher confidence in mimicking multicellular systems. Channels more closely resemble veins and bile-ducts present in the liver. (iii) Printed 3D structures. Most precisely imitates the microstructure in the liver. Complexity and precision favors morphology and cell growth.

In Figure 11, one can see the stepwise increase in cholangiocarcinoma model complexity, starting from simple 2D culture to co-culture growth in 3D ECM mimicking hydrogel microchannels. GelMA was used tor microchannel formation in this study, due to the presence of cell-attaching peptide motifs and matrix metalloproteases.

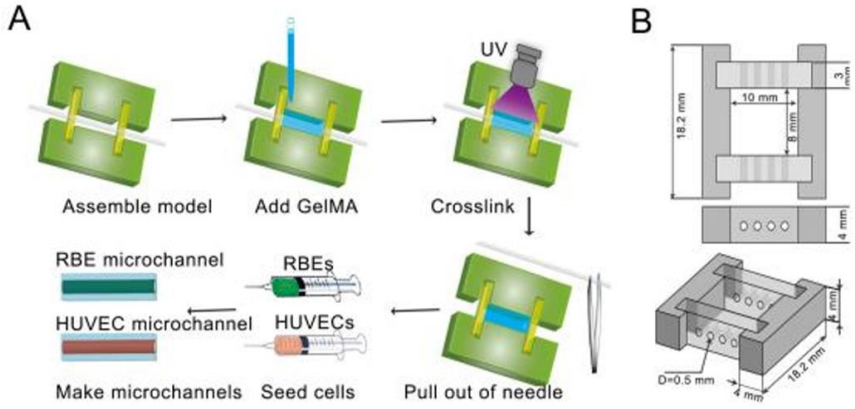


Figure 12: GelMA based channels. (A) GelMA microchannel chip creation, workflow diagram (B) A schematic of the four-channel chip's mold dimensions.

A schematic representation of the channel creation can be seen in Figure 12A and the mold and its dimension can be seen in Figure 12B.

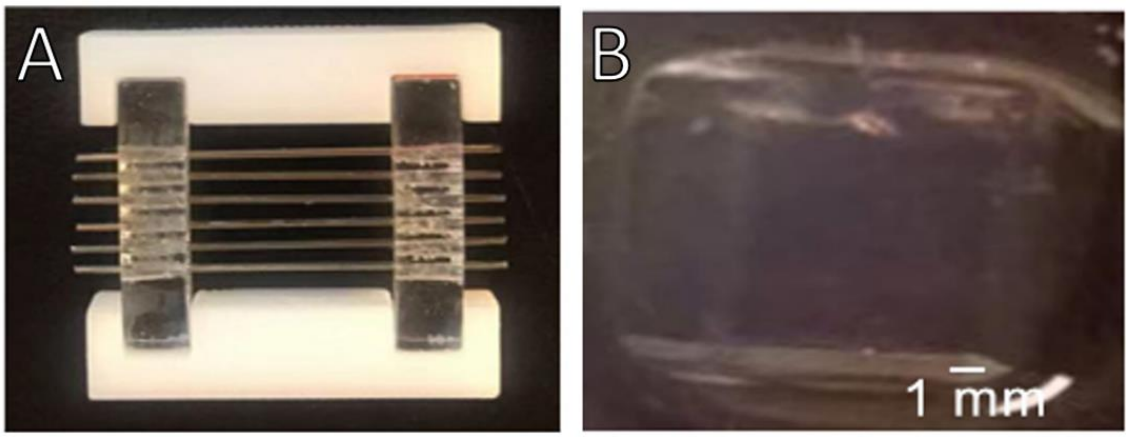


Figure 13: Fabrication of GelMA based functional microchannels (A) An image of the assembled mold used to pour GelMA into, to in the end produce the GelMA chip. (B) The GelMA based cholangiocarcinoma model after crosslinking under UV and disassembly of the mold around. Scale bar 1mm.

The laser cut PMMA mold parts were assembled as can be seen in Figure 13A, the chamber's dimensions were 8mm in width, 10mm in depth and 4.3mm in height leading to a total volume of 344µL. GelMA was added and crosslinked under UV light. The needles were pulled out, leaving hollow microchannel structures. The formed 3D construct can be seen in Figure 13B. The scaffolds were placed in medium for 2h, for cell seeding. Afterwards, the RBE and HUVEC cells were seeded within the microchannels at a concentration of 1x10^7 cells/mL. The microchannels were flipped every half hour for the first two hours for better distribution. Afterwards, the cells were grown until they were confluent and surrounded the whole microchannel. The channel at confluency under a bright light microscope can be seen in Figure 14.

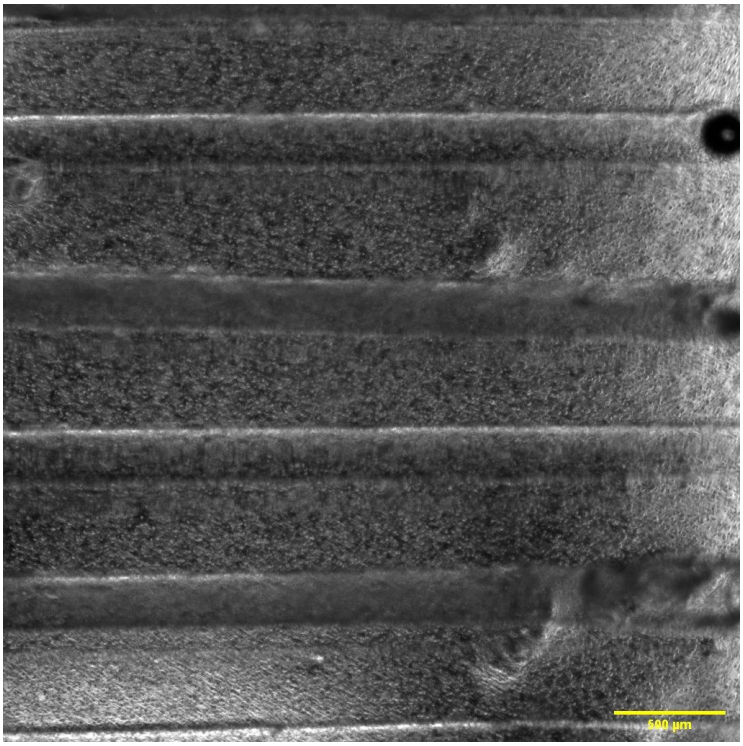


Figure 14: 4-channel GelMA chip with RBE, HUVEC and Hep-G2 under bright light microscope. 2x objective. Scale bar 500µm.

For optimization of spreading and cell adhesion in the microchannels, pork and fish-derived GelMA with various degrees of methacryloyl substitution (high at 90% or medium at 61%) were used to fabricate microchannel chips. After treating with RBE medium for 2h, they were placed in petri dishes and injected with RBE cells. After incubation for 24h to let the cells adhere, morphology and adhesion of RBEs were analyzed under the microscope. Cells in microchannels with low concentration of either fish or pork GelMA, attached poorly and were rounded of. However, when placed in higher concentrated GelMA of both pork and fish, cells spread and showed higher attachment.

Pork and higher concentrations of fish GelMA have shown higher compressive modulus, which leads to an association of stiffness of GelMA with cell adhesion. In other words, a relatively higher compressive modulus supports growth of RBE on the regarding surface of the material. In previous tests it was reported that the normal liver stiffness modulus is under 6kPa (Mueller & Sandrin, 2010). Therefore, 5–7% pork, as well as fish GelMA were chosen for cell support.

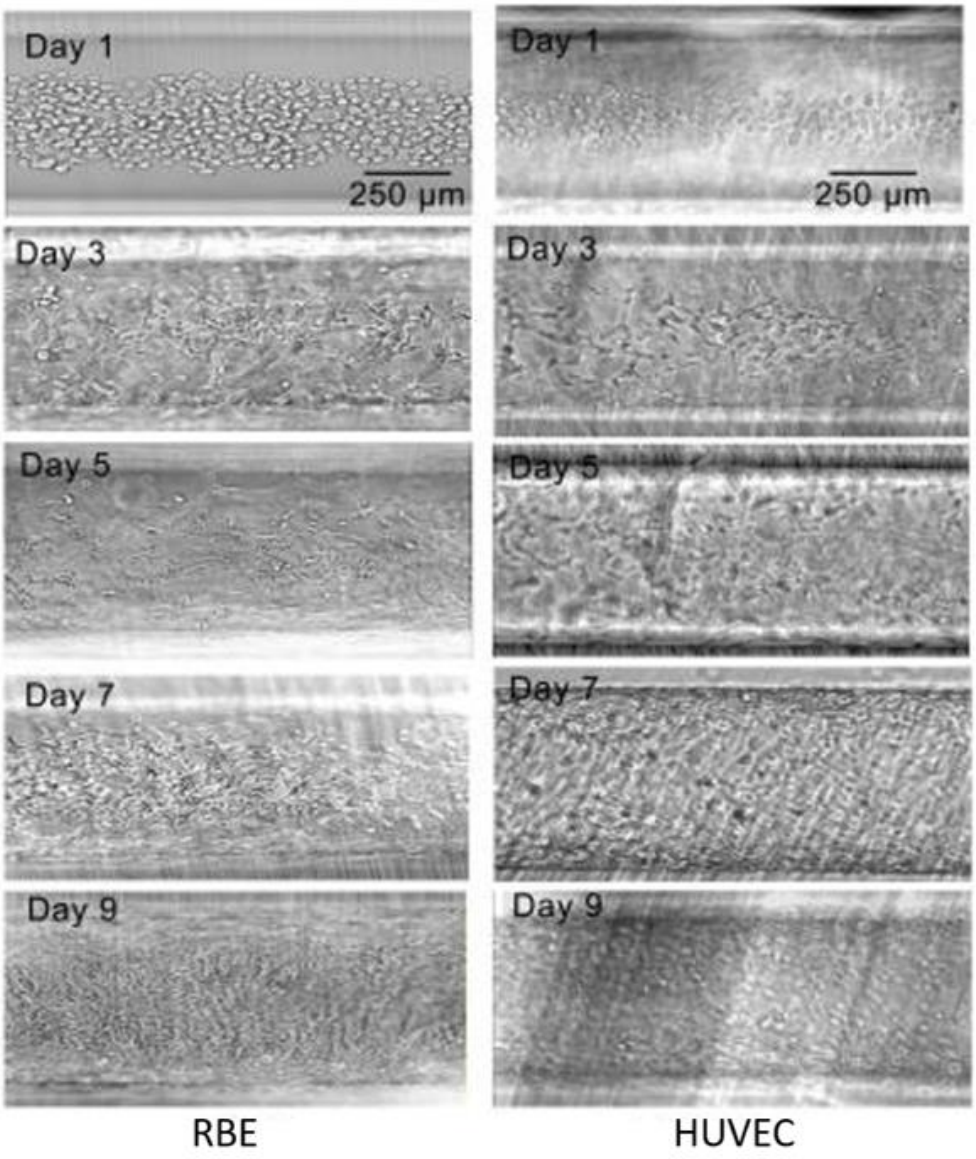


Figure 15. Cell growth of RBE (left) and HUVEC (right) cells in 5% pork-M-GelMA over nine days taken under bright light microscope at 10X magnification. Scale bar 250µm.

To test cell growth further, HUVECs and RBEs were seeded in microchannels with 5% pork-M-GelMA. In Figure 15, it can be seen that on the first day the RBE and HUVEC cells were clustered and round at the bottom of the microchannel. In the following days, they were able to proliferate and spread. At day nine they covered most of the microchannel's surface area.

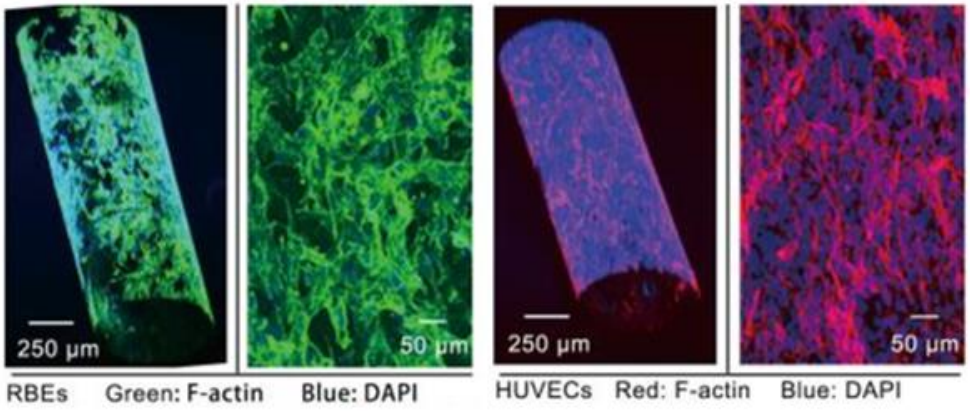


Figure 16: Confocal microscopy of RBE and HUVEC cells in microchannels. Immunostaining of RBEs F-actin in green and HUVCEs F-actin in red, with cell nuclei DAPI staining in blue. Scale bars of 250 and 50µm.

After nine days, the 3D vessel (HUVEC) and cholangiocarcinoma (RBE) microchannels were identified by F-actin and 4′,6-Diamidin-2-phenylindol (DAPI) staining, which can be seen in Figure 16. This confirmed the cells compatibility with the microchannel's material, GelMA.

## 3.2 3D Cholangiocarcinoma-on-a-Chip and triculture system

The cholangiocarcinoma microenvironment is a multicellular and complex functional compartment. Particularly when put together as a copious desmoplastic reaction, this could affect the invasive and proliferative abilities of the cancer cells involved. When compared to 2D monoculture, 3D co-culture with included hepatocytes and vessel cells is a significant step towards mimicking the cholangiocarcinoma's complexity. Cells found in 2D monoculture are limited in x-y interaction within the petri dish, 3D co-culture however got better in representing crosstalk and cellular response which occurs *in vivo*.

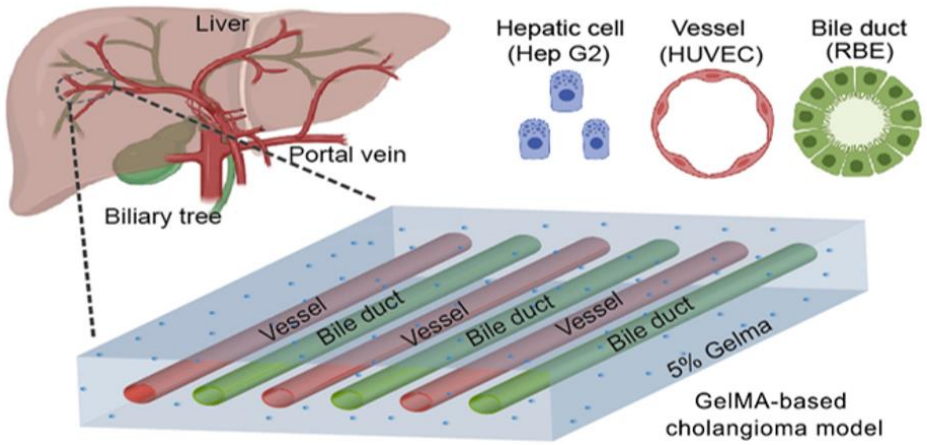


Figure 17. Diagram showing the model's biomimetic acceptability. The model recreates the interplay between hepatic cells, blood vessels, and bile ducts.

As shown in Figure 17, the biliary tree in the liver, which is lined by cholangiocytes, runs side by side with branches from the portal vein and hepatic artery. For modelling the cellular interaction and local microenvironment, the 6-microchannel cholangiocarcinoma-on-a-chip system with co-culture was developed, which is also depicted as model in Figure17.

Those chips were made from 5% pork GelMA with embedded HepG2 cells to simulate the parenchyma of the liver. In order to mimic vascularization and bile ducts, three HUVEC and three RBE microchannels were alternately arrayed in one chip. This way, RBEs could adhere, migrate and proliferate in a microenvironment which grew multiple cells to interact with.

When considering that the various single cultures were integrated into one triculture, the composition of the medium used had to be adjusted accordingly. In the first try, HepG2/HUVEC/RBE media were mixed in a 1:1:1 ratio, however, HUVEC cells died off after only 72h of culture (data not shown). To aid growth of HUVEC cells, vascular endothelial growth factor (VEGF) was added to the co-culture media mixture at a concentration of 10ng/mL.

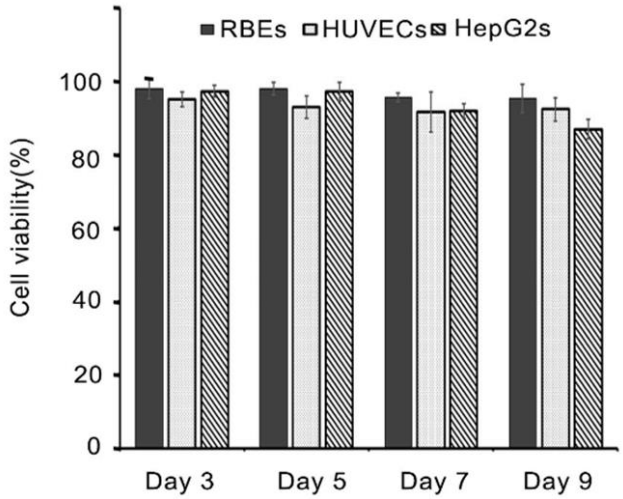


Figure 18: Cell viability of RBE, HUVEC and HepG2 cells during the first nine days in co-culture. Determined by a live/dead assay.

As can be seen in Figure 18, the viability assay illustrates that with the addition of VEGF more than 90% of the HUVEC cells were attached and viable inside the microchannels. Additionally, also more than 90% of both HepG2 and RBE cells could be observed in the GelMA construct throughout the whole nine days of co-culture.

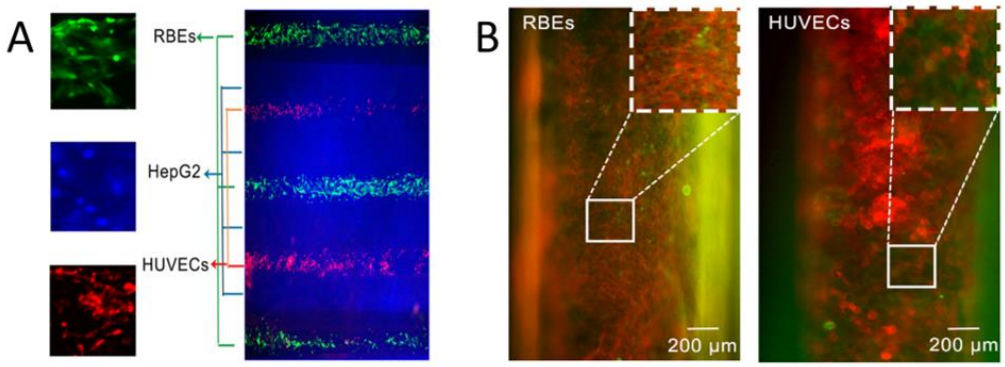


Figure 19: Co-culture 3D cholangiocarcinoma model with three different cell types. (A) The GelMA chip with RBE-LifeAct_EGFP (green) and HUVEC-LifeAct-RFP (red) shown in alternating microchannels and the surrounding GelMA construct with HepG2 embedded marked via cell tracker (blue). (B) Images of confocal microscopy showing the specific HUVEC and RBE markers. RBEs (left; CK17 in green; F-actin in red) and HUVECs (right; CD31 in green; F-actin in red).

For visualization of the cells within the microchannels, a LifeAct-EGFP overexpression in RBEs (RBE-LifeAct-EGFP), as well as LifeAct-RFP overexpression in HUVECs (HUVEC-LifeAct-RFP), were carried out by lentiviral transfection. For tracking of HepG2 location and adhesion, they were labelled with CellTracker Blue just before integration into the chips. From Figure 19A, one can see that after four days of co-

culture, RBE-LifeAct-EGFP and HUVEC-LifeAct-RFP grew well in the alternative and separated microchannels, HepG2-Blue were round and distributed within the matrix. Dual-labelling immunofluorescence images were taken. As can be seen in Figure 19B, the epithelial-specific marker (CK17, green in left panel) was greatly expressed in RBE. F-actin (shown in red) indicates tight cell-cell connection between RBEs. Additionally, another epithelial specific marker (CD31, green in right panel) was greatly expressed in HUVEC. F-actin (shown in red) indicates high adhesion of HUVECs. This 6-microchannel model for cholangiocarcinoma realized crosstalking among the integrated three cell lines and was able to reconstruct the microenvironment present at cholangiocarcinoma *in vivo*.

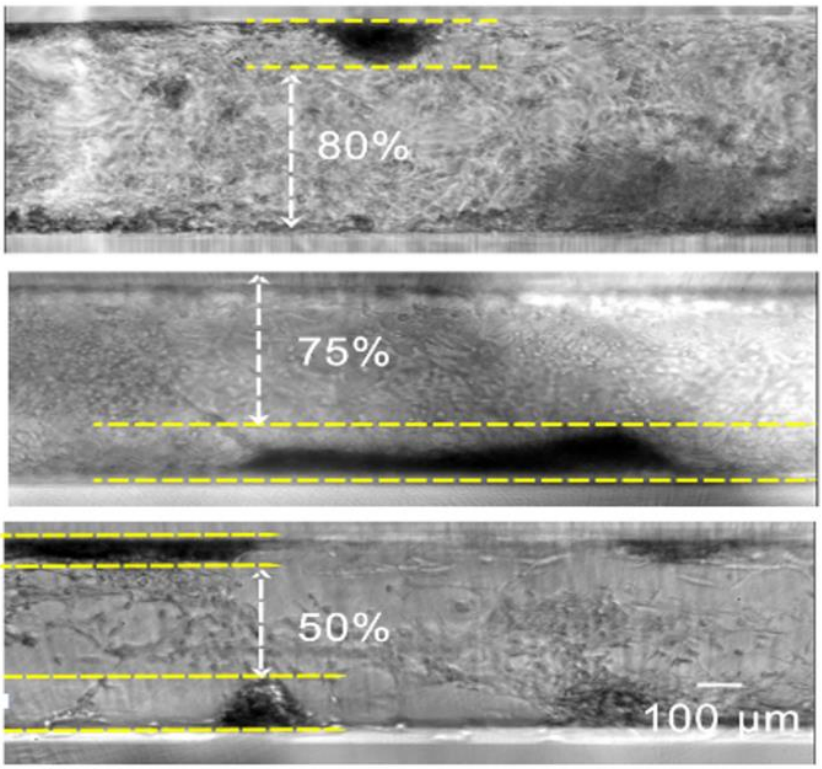


Figure 20: Biliary structures mimicking cholangioma. Image taken under bright light microscope showing the microchannel structure of a cholangiocarcinoma-on-a-chip model. The structure was induced by cholangioma-like hyperproliferation along the walls of the microchannel.

RBE hyperproliferation in these cholangiocarcinoma-on-a-chip models could be observed when incubated for over one week, as can be seen in Figure 20. This inferred the microchannel, and therefore the microenvironment of the models where this was the case had a higher potential for cholangiocarcinoma cell growing and hyperplasia of the tumor. Therefore, this mimicked the biliary duct structure when undergoing transition to cholangiocarcinoma well.

## 3.3 Design & assessment of 3D printed chip

GelMA based 3D digital light printing, with the help of a DMD to create a photomask, enabled a selective and rapid solidification to generate a well-defined crosslinked 3D model.

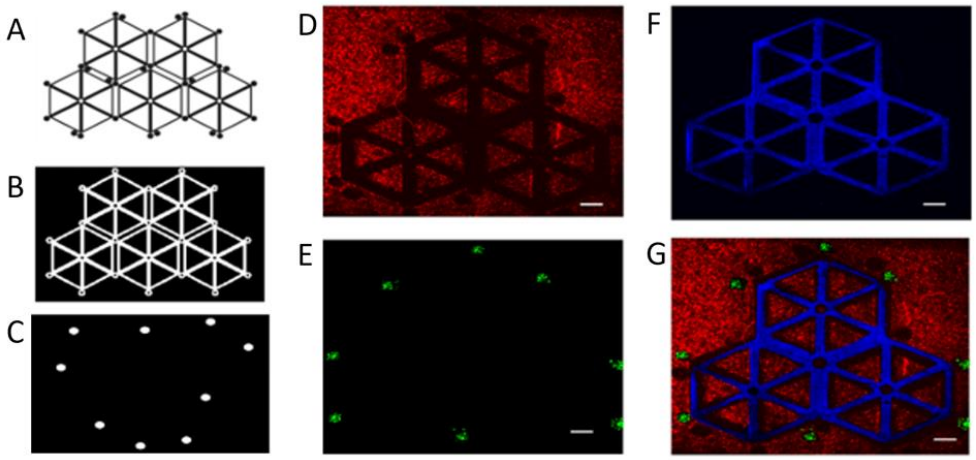


Figure 21: A 3D-bioprinting approach for Cholangioma-on-a-Chip in three steps. (A) Greyscale digital mask for polymerizing lobule structure. (B) Greyscale digital mask for polymerizing vascular structure. (C) Greyscale digital mask for polymerizing bile duct structure. (A–C) The white parts of the digital mask represent the light reflecting patterns for polymerization. (D–G) Images taken with fluorescence microscope. (D) HepG2 fluorescently labelled in red, within a 5% GelMA (E) RBEs fluorescently labelled in green (F) HUVECs fluorescently labelled in blue (G) Merged image of D to F. Scale bars 100µm.

To generate a cholangiocarcinoma-on-a-chip model which represents the cell composition and architecture in the native tissue, the first step was to encapsulate HepG2 (fluorescently labelled, red), HUVEC (fluorescently labelled, blue), and RBE (fluorescently labelled, green) in patterns which mimic the hepatic lobule structure. This was achieved by hydrogel matrix photopolymerization and can be seen in Figure 21 D–G. To simulate the anatomical structures of hepatocytes, vessels, and cholangiocarcinoma, three correspondent patterns were designed as grayscale digital masks, which can be seen in Figure 21 A–C. The three types of cells were spatially patterned by applying these in a three-step process. First, the layer of hepatic cells was created, followed by the vascular and lastly the bile duct layer. The chips created in this process successfully patterned all three kinds of cells and contained an array of liver lobule structures, as can be seen in Figure 21G.

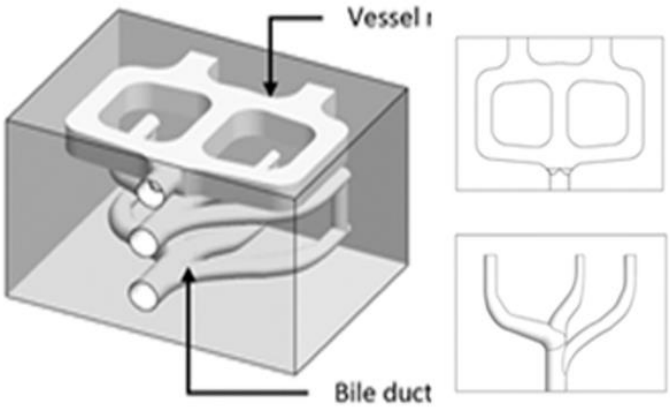


Figure 22:Computer model of separately layered blood vessels and bile duct within the chip.

Even though this three-layer design displays the feasibility of interaction between the three cell lines, introduction of extra structural features into the cholangiocarcinoma-on-a-chip model would model cholangiocarcinoma even better, an example of which is shown in Figure 22. Especially, the addition of branching networks to the 3D chips. Therefore, functional and structural separated microchannels were embedded into the chip.

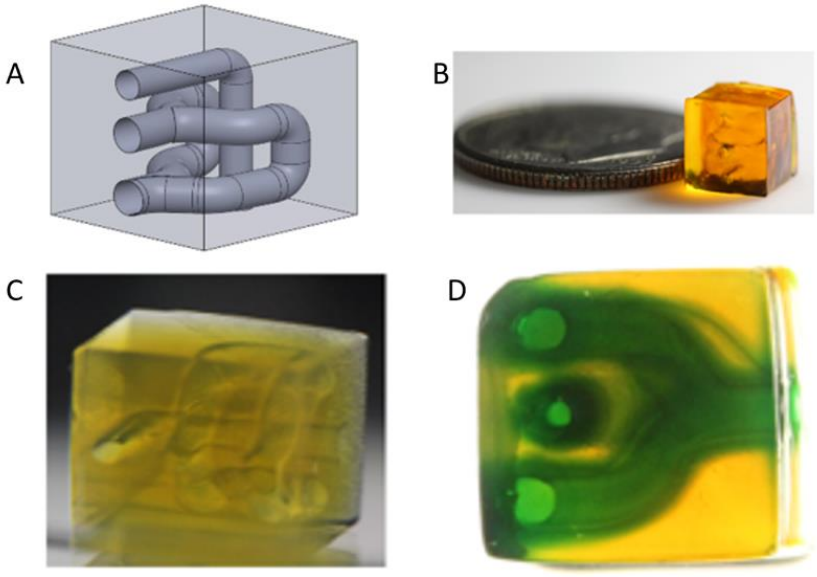


Figure 23:The entwined 3D cholangiocarcinoma-on-a-chip model. (A) Computer model of an entwined structure with Y-shaped bile ducts and L-shaped blood vessels. (B) 3D cholangiocarcinoma-on-a-chip next to an American quarter coin for size comparison. (C) Close up picture of the construct with open channels (D) Printed structure with green food dye injected into the channels to demonstrate connectivity of the channels.

In Figure 23, the resin-based chips can be seen. As the pictures show, the chips provided a great model of the cholangiocarcinoma structure including blood vessels and bile ducts within the surrounding liver.

## 3.4 Difference in 2D and 3D cholangiocarcinoma cells gene expression

It is thought that tumor cells in 2D culture have differences in gene expression and splicing, as well as topology and biochemistry. Therefore, optimization of these conditions and a stronger focus on 3D culture and co-culture of different cell types, may allow for a better understanding.

Consistently, we could see that RBEs in 2D culture, when compared to 3D cholangiocarcinoma chips, induced stronger cell adhesion. This implied that the cells in the two different setups of 2D monoculture versus 3D triculture would lead to differences in gene expression. Therefore, fabricated chips cultivated with RBE, HUVEC and HepG2 until surrounding the channels, were send to an RNA-sequencing facility, to identify the differences in gene expression between 2D and 3D culture.

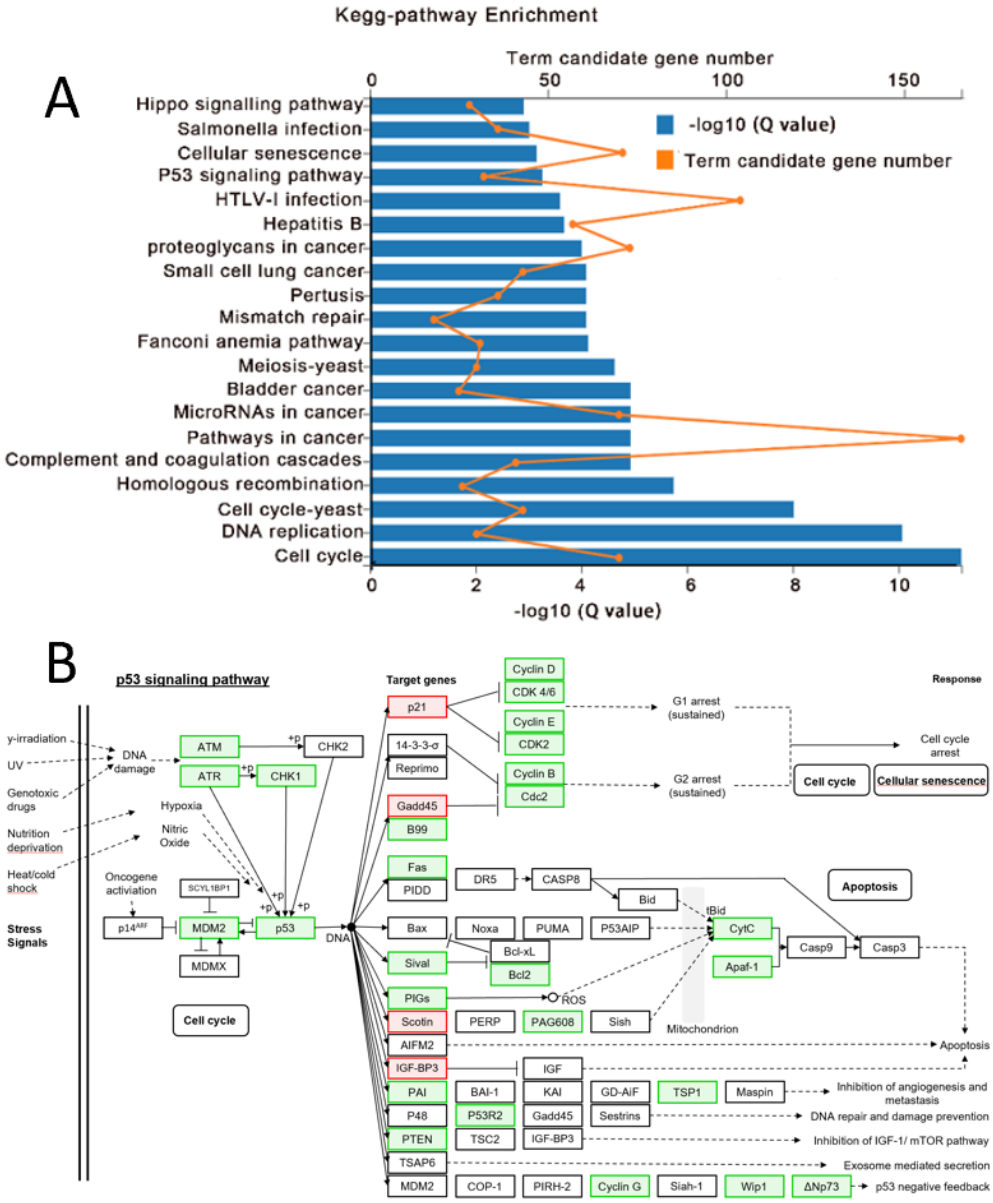


Figure 24. RNA-seq results of comparison between RBEs in 2D monoculture and 3D cholangiocarcinoma-on-a-chip triculture. (A) KEGG pathway analysis. The main KEGG pathways where over 500 changed genes are included in are shown. (B) Differences in p53 signaling pathway gene expression. Green upregulated in 3D model. Red downregulated in 3D model.

The results of the RNA sequencing when doing a pathway analysis show that many of the pathways which are upregulated in our 3D model (see Figure 24) have a link to cancer as for example the p53 pathway. As a prime example, we visualized the genes upregulated and downregulated within the p53-pathway (see Figure 24B). Green boxes are upregulated genes of the 3D model when compared to the usual 2D monoculture model and the red boxes are downregulated genes in the 3D model when compared to

the 2D model. Many of the key players in the p53 pathway are affected by the differences in culturing methods.

The results from the RNA-seq confirm that the cholangiocarcinoma cells cultured in the GelMA-based chip with HepG2 and HUVECs, achieved more stimulation form the microenvironment in the culture and therefore can better mimic the situation *in vivo*. This possibly makes the cholangiocarcinoma-on-a-chip models a better solution for anti-tumor drug screening.

## 3.5 Cholangiocarcinoma cell sensitization to cyclophosphamide

Cyclophosphamide is simply absorbed and converted by the liver's cytochrome P450 system to its active metabolites which includes 4-hydroxycyclophosphamide (Appel & Appel, 2008).

For testing the hypothesis that cytochrome P450 metabolism is present in 3D cholangiocarcinoma-on-a-chip models and not in 2D monoculture, a simple cell counting experiment was performed on both with a CCK-8 kit.

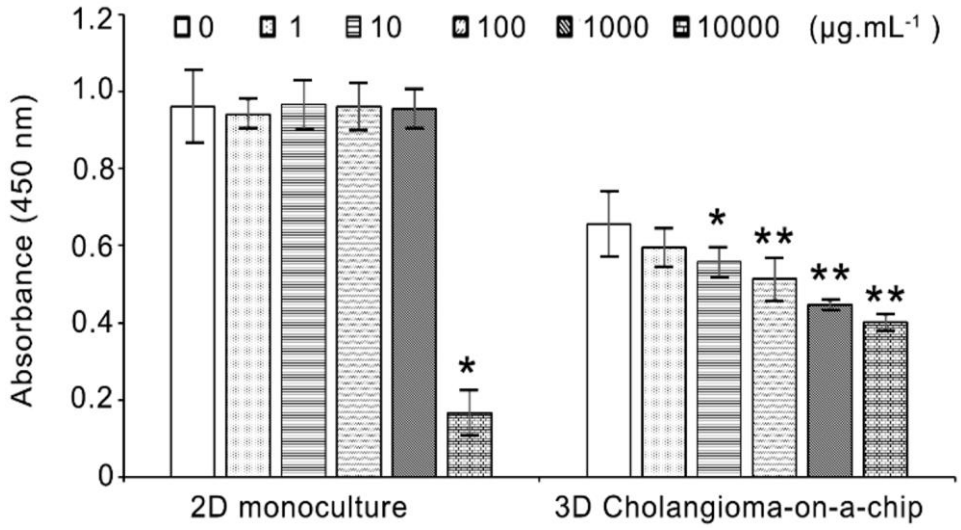


Figure 25: Cytotoxicity analysis with cyclophosphamide in 2D and 3D models by cell counting experiment. On the x-axis 2D monoculture and 3D triculture are displayed with treatment of cyclophosphamide in different concentrations. The treatment with different concentrations is shown with different patterns. The viability of the cells is in direct link with the absorbance at 450nm. Therefore, in 2D monoculture when treated with cyclophosphamide up until 1000μg/mL, no significant decrease in cell viability can be seen. On the contrary, in 3D triculture the effects of cyclophosphamide are already visible in low concentrations. Data are shown as mean ± standard deviation. *P<0.05 **P<0.01 versus each 0μg/mL group.

The cytotoxic assay shows that when RBE is handled in 2D monoculture, the toxicity of cyclophosphamide is rather low, even at high concentrations. However, when added to

the cholangiocarcinoma-on-a-chip model, a toxic effect can clearly be seen, even at low concentrations (see Figure 25). For further testing, the culture mediums were checked for 4-hydroxycyclophosphamide, which was found in higher concentration in cholangiocarcinoma-on-a-chip models (data not shown). This indicates that cyclophosphamide was possibly transformed by HepG2 cells in the co-culture system. Therefore, the cholangiocarcinoma-on-a-chip model is a conceivably better approach when studying new treatment strategies and new biomarkers and will bring us a step closer to personalized medicine.

# 4. DISCUSSION

## 4.1 GelMA-based 3D functional microchannels

For our study, we wanted to show an increased complexity. Therefore, we started with state of the art 2D culture as a starting point which we can later reference to. To start into 3D culture, GelMA was used due to its resemblance of the native extracellular matrix. GelMA has matrix metalloproteinase responsive and cell attaching peptide motifs (Yue et al., 2015). The GelMA was utilized in forming a microchannel for the cells to grow on.

A mold, laser-cut out of PMMA, for forming the microchannels with needles was created successfully with the dimensions requested. With the mold, a GelMA construct could be made as can be seen in Figure 13. With the successful creation of the GelMA construct, the cells were added and grown. The cells grew well on the created chip and could be seen in high numbers under a microscope, surrounding also the microchannels. For spreading and cell adhesion optimization, different methacryloyl substitution degrees have been tried. They were analyzed by growing RBE and looking under the microscope. Higher spread and attachment could be observed with the higher concentrated GelMA. This higher concentrated GelMA has also shown a higher compressive modulus, which leads to the connection between better cell adhesion with stiffness of GelMA. Therefore, to support the growth of RBE on the material, 5–7% GelMA was used for further experiments. To see this improvement, the RBE and HUVEC cells were grown in 5% GelMA microchannels for nine days and fluorescently labelled. This showed that they were able to cover their respective improved microchannel within this time and confirmed the cells' compatibility with the chosen material to work further with.

The possibility of adapting and precisely tune hydrogels for the application at hand provides a valuable tool for the generation of a specific microenvironment. On this ground, GelMA provides the perfect platform for cell cultivation: easily synthesized, low price, transparent (easier monitoring of the cells embedded) and the desired stiffness can be adjusted with concentration. However, the use of GelMA as bioink in bioprinting has to be further explored as the resolution and the maximal height able to be reached is still lacking (Pepelanova et al., 2018).

## 4.2 3D Cholangiocarcinoma-on-a-chip and triculture system

The tumor microenvironment is multicellular and complex. Thus, it might not be enough to look at the unicellular level, as is the case in 2D monoculture. To introduce the microenvironment and see the effects of its proliferative and invasive abilities on the cancer cells within, 3D co-culture of various cell types is a significant step towards better mimicking the tumor's native counterpart. Therefore, to imitate the typical cholangiocarcinoma environment, the addition of liver cells (Hep-G2) and vessel cells (HUVEC) is crucial to simulate cellular responses to the cancer cells and crosstalk (Fabris et al., 2019).

So, a 6-microchannel cholangiocarcinoma-on-a-chip system was created with 5% GelMA as surrounding ECM-support to grow with embedded Hep-G2 cells. To mimic vascularization and bile ducts, three microchannels were alternately seeded with HUVEC and RBE cells. Therefore, RBE cells could adhere, migrate and proliferate in a way which represents the *in vivo* situation much better. This triculture of Hep-G2, HUVEC and RBE cells needed a special media composition as all the different cell needs had to be taken into account. Therefore, a mixture was created with a media ratio of 1:1:1 of all three cells, whereas VEGF had to be added in a concentration of 10ng/mL as otherwise, HUVECs died off after only 72h in culture. With this media composition we were able to cultivate all three cell types inside the chips for nine days with good attachment and viability. This was a big milestone for the project as the best 3D renders for microchannels are worth nothing when the cells are not being able to be kept alive for the time period which the cells would need to be further experiment on.

Visualization of the cells within the microchannels was achieved by lentiviral transfection of RBE with RBE-LifeAct-EGFP and HUVEC with HUVEC-LifeAct-RFP. This was performed by the lab before my arrival. HepG2 cells were tracked for location and adhesion by CellTracker. This made it possible to see and differentiate between cells within the chips. Then it could be seen that all cells were viable and within their seeded segments, which can be seen in Figure 19A. Another phenomenon which could be seen in this chip setting was the RBE's hyperproliferation. After one week of incubation, the RBE cells had a higher potential for cell growth and tumor hyperplasia. This is a common structure when undergoing cholangiocarcinoma transition (DeMorrow et al., 2014) and is therefore a good indication that our model mimicked the biliary duct when cholangiocarcinoma is present.

## 4.3 Design & assessment of 3D-bioprinted chip

For 3D printing with GelMA, a digital light printer was used, and 2 models were created. The first cholangiocarcinoma-on-a-chip model was inspired by the hepatic lobule structure. Therefore, hepatocytes, vessels and cholangiocarcinoma cells were printed with correspondent patterns layer by layer in the following order: hepatic cells, vascular cells and bile duct/ cholangiocarcinoma cells. This created one full liver lobule structure which can be seen in Figure 21G. This design displays the interaction feasibility between the cell lines included and constitutes a good model for further exploration. However, this does not include any structural features, whatsoever. Therefore, for a second model we chose to add branching networks as they would naturally occur in the liver section we wanted to mimic.

This model with added branching networks was realized as prototype using resin as can be seen in Figure 23. In the future, the aim will be to recreate this model using GelMA. The structure of this model (as shown in Figure 23) included a Y-shaped bile duct and a L-shaped blood vessel and therefore perfectly resembles the section of the liver the cholangiocarcinoma would reside in. Additionally, the introduction of vessel structures would allow for the introduction of microfluidic capabilities and hence perfusion of these microchannels. Also, these chips could then be interconnected with other organ-on-a-chips such as kidney or gut, to further see interactions between not only the cells within the cholangiocarcinoma-on-a-chip, but with surrounding organs connected by the blood stream (Kimura, Sakai, & Fujii, 2018).

## 4.4 Difference in 2D and 3D cholangiocarcinoma cell gene expression

The simplicity of 2D-monoculture does not allow intercellular crosstalk, which is a crucial part of many cellular processes (Baghban et al., 2020). Consequently, it is likely that tumor cells behave differently depending on the used culture system. One of the many aspects that seems to be affected by the choice of model used is gene expression levels (Vantangoli, Madnick, Huse, Weston, & Boekelheide, 2015). Therefore, it was investigated in the presented work, how gene expression levels differ between the used 2D-monoculture and the 3D-triculture system.

The gene expression levels of RBE cells in the different culturing systems were compared using RNA-sequencing. The pathway analysis of this RNA-sequencing shows that many genes which are upregulated in the 3D model are linked to pathways of cancer like the p53 pathway. Mutation of p53 is among the most frequent

encountered genetic aberration in native cholangiocarcinoma and plays a crucial role in the carcinogenesis of cholangiocarcinoma (Liu et al., 2006). This supports our initial impetus that cholangiocarcinoma cells which are cultivated in our GelMA chips with HUVEC and HepG2, got more stimulation from their surrounding microenvironment and consequently better mimic the *in vivo* situation.

## 4.5 Cholangiocarcinoma cell sensitization to cyclophosphamide

Cyclophosphamide is an alkylating drug often used in the treatment of cancers such as leukemia, breast cancer and lymphoma. In the liver, cyclophosphamide is absorbed and further transformed into 4-hydroxycyclophophamide by CYP450 (de Jonge, Huitema, Rodenhuis, & Beijnen, 2005). Promisingly, the cholangiocarcinoma-on-a-chip model displayed the same response to the chemotherapeutic agent. The cyclophosphamide cytotoxic assay showed the tri-culture system's clear advantage: while the 2D monoculture models showed a weakened response to the compound, the 3D triculture model showed an obvious increase in cell death corresponding to the increase in cyclophosphamide concentration administered (Figure 25). Additionally, a higher presence of 4-hydroxcyclophosphamide in the cholangiocarcinoma-on-a-chip model's medium implies that presumably Hep-G2 metabolically processed the hepatotoxin. These results propose that, compared to the 2D monoculture, the 3D cholangiocarcinoma-on-chip model can more precisely mimic the response of *in vivo* cholangiocarcinoma to potential treatments. Therefore, it poses as better model for drug discovery.

## 4.6 Conclusion

To conclude, this project offers a convenient, cost-effective and accurate cholangiocarcinoma-on-a-chip system for a variety of applications such as drug discovery, personalized medicine and functional studies. The produced chip consists of photoinitiated GelMA with embedded Hep-G2 cells, within which were alternating microchannels of HUVEC and RBE cells. This chip was submerged into optimized triculture medium. The structure and cellular environment were designed to mimic real liver conditions, while also being suitable for 3D bioprinting. The experiments performed showed that the platform is an adequate alternative for drug screening purposes, without compromising in accessibility and predictive value, therefore being able to be used in evaluation of personalized treatment.

At the moment, 2D monoculture and xenografts from patients are the two most prominent models, each with their own disadvantages. 2D monoculture lacks the

microenvironment and architecture to accurately mimic the *in vivo* cell responses; these 2D monoculture models show an oversimplified architecture, disturbance in cell interaction, morphology which is not representative of the disease which it should mimic, and overall a culture format which negatively impacts expression, response and cell growth (Kapałczyńska et al., 2018; Stock et al., 2016). On the other side of the spectrum are xenografts derived from patients, because while more authentic, they are also very expensive, time-consuming, and complex in handling. This makes patient-derived xenografts inconvenient for functional studies (Wan, Neumann, & LeDuc, 2020). Consequently, 3D co-culture has been suggested to be the missing link to facilitate understanding of cancer therapies (Kapałczyńska et al., 2018).

By carefully mimicking the cellular microenvironment and structure of cholangiocarcinoma, with the respective biochemical and mechanical cues, the system created in this project can produce a more exact representation. This can be seen when looking at the presented data of differential gene expression and the cyclophosphamide cytotoxic assay.

The developed methods for producing these models were simple, cost-effective and fast. The models can easily be replicated with the appropriate materials and molds. The co-culture medium, optimal for the three used cell lines, is an accessible mixture of the media used for the corresponding cell lines, with the addition of VEGF. Further, the feasibility of 3D bioprinting of these models was demonstrated, which allows for easy and swift mass production and perfusion, to test different hypotheses. The models were produced with photoinitiated GelMA, which offers a range of possible 3D structures. These advances ensure a solid foundation for this platform’s feasibility in further studies.

The chip has demonstrated that it is closely mimicking the *in vivo* conditions of cholangiocarcinoma, granting for complex interplay of biological and structural elements which impact cell responses. The created platform can be further personalized to meet the research needs by using patient-derived cells or producing chips with different configurations.

The focus of future studies should lie on the verification of other chemotherapeutic agents, possible inquiries into the observed hypergrowth of the tumor cells, and the inclusion of patient-derived cells into the chips. The model created in this project will be the beginning of providing new insights in cholangiocarcinoma and personalized care.

## Bibliography


Aizawa, K., Liu, C., Tang, S., Veeramachaneni, S., Hu, K. Q., Smith, D. E., & Wang, X. D. (2016). Tobacco carcinogen induces both lung cancer and non-alcoholic steatohepatitis and hepatocellular carcinomas in ferrets which can be attenuated by lycopene supplementation. *International journal of cancer, 139*(5), 1171-1181.

Alabraba, E., Joshi, H., Bird, N., Griffin, R., Sturgess, R., Stern, N., . . . Davis, R. (2019). Increased multimodality treatment options has improved survival for hepatocellular carcinoma but poor survival for biliary tract cancers remains unchanged. *European Journal of Surgical Oncology, 45*(9), 1660-1667.

Alsibai, K. D., & Meseure, D. (2018). Significance of Tumor Microenvironment Scoring and Immune Biomarkers in Patient Stratification and Cancer Outcomes. *Histopathology: An Update, 11*.

Andersen, J. B., Spee, B., Blechacz, B. R., Avital, I., Komuta, M., Barbour, A., . . . Roberts, L. R. (2012). Genomic and genetic characterization of cholangiocarcinoma identifies therapeutic targets for tyrosine kinase inhibitors. *Gastroenterology, 142*(4), 1021-1031. e1015.

Anguiano, M., Castilla, C., Maška, M., Ederra, C., Peláez, R., Morales, X., . . . Munoz-Barrutia, A. (2017). Characterization of three-dimensional cancer cell migration in mixed collagen-Matrigel scaffolds using microfluidics and image analysis. *PLoS ONE, 12*(2), e0171417.

Antwi, S. O., Eckert, E. C., Sabaque, C. V., Leof, E. R., Hawthorne, K. M., Bamlet, W. R., . . . Petersen, G. M. (2015). Exposure to environmental chemicals and heavy metals, and risk of pancreatic cancer. *Cancer Causes & Control, 26*(11), 1583-1591.

Appel, A. S., & Appel, G. B. (2008). Chapter 10 - Immunosuppressive Agents for the Therapy of Glomerular and Tubulointerstitial Disease. In C. S. Wilcox (Ed.), *Therapy in Nephrology & Hypertension (Third Edition)* (pp. 105-111). Philadelphia: W.B. Saunders.

Ayoubi-Joshaghani, M. H., Dianat-Moghadam, H., Seidi, K., Jahanban-Esfahalan, A., Zare, P., & Jahanban-Esfahlan, R. (2020). Cell-free protein synthesis: The transition from batch reactions to minimal cells and microfluidic devices. *Biotechnology and Bioengineering, 117*(4), 1204-1229. doi:https://doi.org/10.1002/bit.27248

Baghban, R., Roshangar, L., Jahanban-Esfahlan, R., Seidi, K., Ebrahimi-Kalan, A., Jaymand, M., . . . Zare, P. (2020). Tumor microenvironment complexity and therapeutic implications at a glance. *Cell Communication and Signaling, 18*(1), 59. doi:10.1186/s12964-020-0530-4

Banales, J. M., Cardinale, V., Carpino, G., Marzioni, M., Andersen, J. B., Invernizzi, P., . . . Fouassier, L. (2016). Expert consensus document: Cholangiocarcinoma: current knowledge and future perspectives consensus statement from the European Network for the Study of Cholangiocarcinoma (ENS-CCA). *Nature reviews. Gastroenterology & hepatology, 13*(5), 261-280.

Banales, J. M., Marin, J. J. G., Lamarca, A., Rodrigues, P. M., Khan, S. A., Roberts, L. R., . . . Gores, G. J. (2020). Cholangiocarcinoma 2020: the next horizon in mechanisms and management. *Nature Reviews Gastroenterology & Hepatology, 17*(9), 557-588. doi:10.1038/s41575-020-0310-z

Bernal, P. N., Delrot, P., Loterie, D., Li, Y., Malda, J., Moser, C., & Levato, R. (2019). Volumetric Bioprinting of Complex Living-Tissue Constructs within Seconds.

*Advanced Materials, 31*(42), 1904209. doi:https://doi.org/10.1002/adma.201904209

Bileckot, R., Masson, C., Ntsiba, H., Mbongo, J., Biendo, M., Yala, F., & Brégeon, C. (1991). Prospective study of rheumatic manifestations in human immunodeficiency virus infection. Apropos of 26 cases in Congo. *Revue du rhumatisme et des maladies osteo-articulaires, 58*(3), 163-168.

Billiet, T., Vandenhaute, M., Schelfhout, J., Van Vlierberghe, S., & Dubruel, P. (2012). A review of trends and limitations in hydrogel-rapid prototyping for tissue engineering. *Biomaterials, 33*(26), 6020-6041.

Bishop, E. S., Mostafa, S., Pakvasa, M., Luu, H. H., Lee, M. J., Wolf, J. M., . . . Reid, R. R. (2017). 3-D bioprinting technologies in tissue engineering and regenerative medicine: Current and future trends. *Genes & Diseases, 4*(4), 185-195. doi:https://doi.org/10.1016/j.gendis.2017.10.002

Blatt, N. L., Mingaleeva, R. N., Khaiboullina, S., Lombardi, V., & Rizvanov, A. (2013). Application of cell and tissue culture systems for anticancer drug screening. *World Appl. Sci. J, 23*(3), 315-325.

Brunsveld, L., Folmer, B. J. B., Meijer, E. W., & Sijbesma, R. P. (2001). Supramolecular Polymers. *Chemical reviews, 101*(12), 4071-4098. doi:10.1021/cr990125q

Brunt, E., Aishima, S., Clavien, P. A., Fowler, K., Goodman, Z., Gores, G., . . . Komuta, M. (2018). cHCC-CCA: Consensus terminology for primary liver carcinomas with both hepatocytic and cholangiocytic differentation. *Hepatology, 68*(1), 113-126.

Buwalda, S. J., Boere, K. W. M., Dijkstra, P. J., Feijen, J., Vermonden, T., & Hennink, W. E. (2014). Hydrogels in a historical perspective: From simple networks to smart materials. *Journal of Controlled Release, 190*, 254-273. doi:https://doi.org/10.1016/j.jconrel.2014.03.052

Catoira, M. C., Fusaro, L., Di Francesco, D., Ramella, M., & Boccafoschi, F. (2019). Overview of natural hydrogels for regenerative medicine applications. *Journal of Materials Science: Materials in Medicine, 30*(10), 115. doi:10.1007/s10856-019-6318-7

Catros, S., Fricain, J.-C., Guillotin, B., Pippenger, B., Bareille, R., Remy, M., . . . Guillemot, F. (2011). Laser-assisted bioprinting for creating on-demand patterns of human osteoprogenitor cells and nano-hydroxyapatite. *Biofabrication, 3*(2), 025001.

Chen, X. B., Schoenau, , G., & Zhang , W. J. (2002). On the Flow Rate Dynamics in Time-Pressure Dispensing Processes. *Journal of Dynamic Systems, Measurement, and Control, 124*(4), 693-698. doi:10.1115/1.1514058

Chen, L., Xiao, Z., Meng, Y., Zhao, Y., Han, J., Su, G., . . . Dai, J. (2012). The enhancement of cancer stem cell properties of MCF-7 cells in 3D collagen scaffolds for modeling of cancer and anti-cancer drugs. *Biomaterials, 33*(5), 1437-1444.

Chen, X. B. (2006). Modeling of Rotary Screw Fluid Dispensing Processes. *Journal of Electronic Packaging, 129*(2), 172-178. doi:10.1115/1.2721090

Chimene, D., Lennox, K. K., Kaunas, R. R., & Gaharwar, A. K. (2016). Advanced Bioinks for 3D Printing: A Materials Science Perspective. *Ann Biomed Eng, 44*(6), 2090-2102. doi:10.1007/s10439-016-1638-y

Cigudosa, J. C., Parsa, N. Z., Louie, D. C., Filippa, D. A., Jhanwar, S. C., Johansson, B., . . . Chaganti, R. (1999). Cytogenetic analysis of 363 consecutively ascertained diffuse large B-cell lymphomas. *Genes, Chromosomes and Cancer, 25*(2), 123-133.

Clevers, H. (2016). Modeling development and disease with organoids. *Cell, 165*(7), 1586-1597.

Cui, H., Nowicki, M., Fisher, J. P., & Zhang, L. G. (2017). 3D Bioprinting for Organ Regeneration. *Adv Healthc Mater, 6*(1). doi:10.1002/adhm.201601118

Cui, X., Boland, T., D'Lima, D. D., & Lotz, M. K. (2012). Thermal Inkjet Printing in Tissue Engineering and Regenerative Medicine. *Recent Pat. Drug Delivery Formulation, 6*, 149.

Cumberbatch, M. G., Cox, A., Teare, D., & Catto, J. W. (2015). Contemporary occupational carcinogen exposure and bladder cancer: a systematic review and meta-analysis. *JAMA oncology, 1*(9), 1282-1290.

Dai, X., Liu, L., Ouyang, J., Li, X., Zhang, X., Lan, Q., & Xu, T. (2017). Coaxial 3D bioprinting of self-assembled multicellular heterogeneous tumor fibers. *Scientific Reports, 7*(1), 1-11.

Daly, A. C., Cunniffe, G. M., Sathy, B. N., Jeon, O., Alsberg, E., & Kelly, D. J. (2016). 3D Bioprinting of Developmentally Inspired Templates for Whole Bone Organ Engineering. *Advanced Healthcare Materials, 5*(18), 2353-2362. doi:https://doi.org/10.1002/adhm.201600182

de Gruijl, F. R., van Kranen, H. J., & Mullenders, L. H. (2001). UV-induced DNA damage, repair, mutations and oncogenic pathways in skin cancer. *Journal of Photochemistry and Photobiology B: Biology, 63*(1-3), 19-27.

de Jonge, M. E., Huitema, A. D., Rodenhuis, S., & Beijnen, J. H. (2005). Clinical pharmacokinetics of cyclophosphamide. *Clin Pharmacokinet, 44*(11), 1135-1164. doi:10.2165/00003088-200544110-00003

DeMorrow, S., Francis, H., Marzioni, M., Leyva-Illades, D., Han, Y., & Alpini, G. (2014). Cholangiocarcinoma. In L. M. McManus & R. N. Mitchell (Eds.), *Pathobiology of Human Disease* (pp. 1894-1911). San Diego: Academic Press.

Denisenko, T. V., Budkevich, I. N., & Zhivotovsky, B. (2018). Cell death-based treatment of lung adenocarcinoma. *Cell Death Dis, 9*(2), 117. doi:10.1038/s41419-017-0063-y

DeOliveira, M. L., Cunningham, S. C., Cameron, J. L., Kamangar, F., Winter, J. M., Lillemoe, K. D., . . . Schulick, R. D. (2007). Cholangiocarcinoma: thirty-one-year experience with 564 patients at a single institution. *Annals of surgery, 245*(5), 755.

Derakhshanfar, S., Mbeleck, R., Xu, K., Zhang, X., Zhong, W., & Xing, M. (2018). 3D bioprinting for biomedical devices and tissue engineering: A review of recent trends and advances. *Bioactive Materials, 3*(2), 144-156. doi:https://doi.org/10.1016/j.bioactmat.2017.11.008

Derby, B. (2008). Bioprinting: Inkjet Printing Proteins and Hybrid Cell-Containing Materials and Structures. *J. Mater. Chem., 18*, 5717.

Di Bella, C., Fosang, A., Donati, D. M., Wallace, G. G., & Choong, P. F. M. (2015). 3D Bioprinting of Cartilage for Orthopedic Surgeons: Reading between the Lines. *Frontiers in surgery, 2*, 39-39. doi:10.3389/fsurg.2015.00039

Donderwinkel, I., van Hest, J. C. M., & Cameron, N. R. (2017). Bio-inks for 3D bioprinting: recent advances and future prospects. *Polymer Chemistry, 8*(31), 4451-4471. doi:10.1039/C7PY00826K

Dontu, G., Al-Hajj, M., Abdallah, W. M., Clarke, M. F., & Wicha, M. S. (2003). Stem cells in normal breast development and breast cancer. *Cell proliferation, 36*, 59-72.

Fabris, L., Perugorria, M. J., Mertens, J., Björkström, N. K., Cramer, T., Lleo, A., . . . Strazzabosco, M. (2019). The tumour microenvironment and immune milieu of cholangiocarcinoma. *Liver Int, 39 Suppl 1*, 63-78. doi:10.1111/liv.14098

Fisher, R., Pusztai, L., & Swanton, C. (2013). Cancer heterogeneity: implications for targeted therapeutics. *British journal of cancer, 108*(3), 479-485.

Frisch, J., Angenendt, A., Hoth, M., Prates Roma, L., & Lis, A. (2019). STIM-Orai Channels and Reactive Oxygen Species in the Tumor Microenvironment. *Cancers, 11*(4), 457. doi:10.3390/cancers11040457

Gao, G., Yonezawa, T., Hubbell, K., Dai, G., & Cui, X. (2015). Inkjet-bioprinted acrylated peptides and PEG hydrogel with human mesenchymal stem cells promote robust bone and cartilage formation with minimal printhead clogging. *Biotechnol J, 10*(10), 1568-1577.

Gauvin, R., Chen, Y.-C., Lee, J. W., Soman, P., Zorlutuna, P., Nichol, J. W., . . . Khademhosseini, A. (2012). Microfabrication of complex porous tissue engineering scaffolds using 3D projection stereolithography. *Biomaterials, 33*(15), 3824-3834.

Gu, B. K., Choi, D. J., Park, S. J., Kim, M. S., Kang, C. M., & Kim, C. H. (2016). 3-dimensional bioprinting for tissue engineering applications. *Biomater Res, 20*, 12. doi:10.1186/s40824-016-0058-2

Gu, Z., Fu, J., Lin, H., & He, Y. (2020). Development of 3D bioprinting: From printing methods to biomedical applications. *Asian Journal of Pharmaceutical Sciences, 15*(5), 529-557. doi:https://doi.org/10.1016/j.ajps.2019.11.003

Gudapati, H., Dey, M., & Ozbolat, I. (2016). A Comprehensive Review on Droplet-Based Bioprinting: Past, Present and Future. *Biomaterials, 102*, 20.

Guillemot, F., Souquet, A., Catros, S., & Guillotin, B. (2010). Laser-assisted cell printing: principle, physical parameters versus cell fate and perspectives in tissue engineering. *Nanomedicine, 5*(3), 507-515.

Guillemot, F., Souquet, A., Catros, S., Guillotin, B., Lopez, J., Faucon, M., . . . Bellance, S. (2010). High-throughput laser printing of cells and biomaterials for tissue engineering. *Acta Biomaterialia, 6*(7), 2494-2500.

Hanahan, D., & Coussens, L. M. (2012). Accessories to the crime: functions of cells recruited to the tumor microenvironment. *Cancer cell, 21*(3), 309-322.

Hassanpour, S. H., & Dehghani, M. (2017). Review of cancer from perspective of molecular. *Journal of Cancer Research and Practice, 4*(4), 127-129. doi:https://doi.org/10.1016/j.jcrpr.2017.07.001

He, Y., Yang, F., Zhao, H., Gao, Q., Xia, B., & Fu, J. (2016). Research on the printability of hydrogels in 3D bioprinting. *Scientific Reports, 6*, 29977-29977. doi:10.1038/srep29977

Holbeck, S. L., Camalier, R., Crowell, J. A., Govindharajulu, J. P., Hollingshead, M., Anderson, L. W., . . . Wilsker, D. (2017). The National Cancer Institute ALMANAC: a comprehensive screening resource for the detection of anticancer drug pairs with enhanced therapeutic activity. *Cancer research, 77*(13), 3564-3576.

Holzl, K., Lin, S., Tytgat, L., Van Vlierberghe, S., Gu, L., & Ovsianikov, A. Bioink properties before, during and after 3D bioprinting. Biofabrication. 2016; 8 (3): 032002.

Hu, J. L., Todhunter, M. E., LaBarge, M. A., & Gartner, Z. J. (2018). Opportunities for organoids as new models of aging. *Journal of Cell Biology, 217*(1), 39-50.

Imamura, Y., Mukohara, T., Shimono, Y., Funakoshi, Y., Chayahara, N., Toyoda, M., . . . Nakatsura, T. (2015). Comparison of 2D-and 3D-culture models as drug-testing platforms in breast cancer. *Oncology reports, 33*(4), 1837-1843.

Iram, D., Riaz, R. a., & Iqbal, R. (2019). *3D Bioprinting: An attractive alternative to traditional organ transplantation*.

Iwanaga, S., Saito, N., Sanae, H., & Nakamura, M. (2013). Facile Fabrication of Uniform Size-Controlled Microparticles and Potentiality for Tandem Drug Delivery System of Micro/Nanoparticles. *Colloids Surf., B, 109*, 301.

Jahanban-Esfahlan, R., Seidi, K., Manjili, M. H., Jahanban-Esfahlan, A., Javaheri, T., & Zare, P. (2019). Tumor cell dormancy: threat or opportunity in the fight against Cancer. *Cancers, 11*(8), 1207.

Jahanban-Esfahlan, R., Seidi, K., Monhemi, H., Adli, A. D. F., Minofar, B., Zare, P., . . . Abbasi, M. M. (2017). RGD delivery of truncated coagulase to tumor vasculature affords local thrombotic activity to induce infarction of tumors in mice. *Scientific Reports, 7*(1), 1-14.

Jahanban-Esfahlan, R., Seidi, K., & Zarghami, N. (2017). Tumor vascular infarction: prospects and challenges. *International journal of hematology, 105*(3), 244-256.

Jahanban-Esfahlan, R., de la Guardia, M., Ahmadi, D., & Yousefi, B. (2018). Modulating tumor hypoxia by nanomedicine for effective cancer therapy. *Journal of cellular physiology, 233*(3), 2019-2031.

Jahanban-Esfahlan, R., Seidi, K., Banimohamad-Shotorbani, B., Jahanban-Esfahlan, A., & Yousefi, B. (2018). Combination of nanotechnology with vascular targeting agents for effective cancer therapy. *Journal of cellular physiology, 233*(4), 2982-2992.

Jana, S., & Lerman, A. (2015). Bioprinting a cardiac valve. *Biotechnology advances, 33*(8), 1503-1521.

Jang, J. (2017). 3D Bioprinting and In Vitro Cardiovascular Tissue Modeling. *Bioengineering (Basel, Switzerland), 4*(3), 71. doi:10.3390/bioengineering4030071

Kamisuki, S., Hagata, T., Tezuka, C., Nose, Y., Fujii, M., & Atobe, M. (1998, 25-29 Jan. 1998). *A low power, small, electrostatically-driven commercial inkjet head.* Paper presented at the Proceedings MEMS 98. IEEE. Eleventh Annual International Workshop on Micro Electro Mechanical Systems. An Investigation of Micro Structures, Sensors, Actuators, Machines and Systems (Cat. No.98CH36176.

Kamsa-ard, S., Luvira, V., Suwanrungruang, K., Kamsa-ard, S., Luvira, V., Santong, C., . . . Pairojkul, C. (2020). Cholangiocarcinoma Trends, Incidence, and Relative Survival in Khon Kaen, Thailand From 1989 Through 2013: A Population-Based Cancer Registry Study [J Epidemiol 29 (5)(2019) 197–204]. *Journal of Epidemiology, 30*(2), 108-109.

Kapałczyńska, M., Kolenda, T., Przybyła, W., Zajączkowska, M., Teresiak, A., Filas, V., . . . Lamperska, K. (2018). 2D and 3D cell cultures - a comparison of different types of cancer cell cultures. *Arch Med Sci, 14*(4), 910-919. doi:10.5114/aoms.2016.63743

Kesti, M., Eberhardt, C., Pagliccia, G., Kenkel, D., Grande, D., Boss, A., & Zenobi-Wong, M. (2015). Bioprinting Complex Cartilaginous Structures with Clinically Compliant Biomaterials. *Advanced Functional Materials, 25*(48), 7406-7417. doi:https://doi.org/10.1002/adfm.201503423

Khan, A. S., & Dageforde, L. A. (2019). Cholangiocarcinoma. *Surg Clin North Am, 99*(2), 315-335. doi:10.1016/j.suc.2018.12.004

Kim, M., Mun, H., Sung, C. O., Cho, E. J., Jeon, H.-J., Chun, S.-M., . . . Choi, E. K. (2019). Patient-derived lung cancer organoids as in vitro cancer models for therapeutic screening. *Nature communications, 10*(1), 1-15.

Kimura, H., Sakai, Y., & Fujii, T. (2018). Organ/body-on-a-chip based on microfluidic technology for drug discovery. *Drug Metabolism and Pharmacokinetics, 33*(1), 43-48. doi:https://doi.org/10.1016/j.dmpk.2017.11.003

Kitaeva, K. V., Prudnikov, T. S., Gomzikova, M. O., Kletukhina, S. K., James, V., Rizvanov, A. A., & Solovyeva, V. V. (2019). Analysis of the interaction and proliferative activity of adenocarcinoma, peripheral blood mononuclear and mesenchymal stromal cells after co-cultivation in vitro. *BioNanoScience, 9*(2), 502-509.

Kitaeva, K. V., Rutland, C. S., Rizvanov, A. A., & Solovyeva, V. V. (2020). Cell Culture Based in vitro Test Systems for Anticancer Drug Screening. *Frontiers in bioengineering and biotechnology, 8*, 322-322. doi:10.3389/fbioe.2020.00322

Klotz, B. J., Gawlitta, D., Rosenberg, A. J., Malda, J., & Melchels, F. P. (2016). Gelatin-methacryloyl hydrogels: towards biofabrication-based tissue repair. *Trends Biotechnol, 34*(5), 394-407.

Koerkamp, B. G., Wiggers, J. K., Allen, P. J., Besselink, M. G., Blumgart, L. H., Busch, O. R., . . . Gouma, D. J. (2015). Recurrence rate and pattern of perihilar cholangiocarcinoma after curative intent resection. *Journal of the American College of Surgeons, 221*(6), 1041-1049.

Kolesky, D. B., Truby, R. L., Gladman, A. S., Busbee, T. A., Homan, K. A., & Lewis, J. A. (2014). 3D Bioprinting of Vascularized, Heterogeneous Cell-Laden Tissue Constructs. *Advanced Materials, 26*(19), 3124-3130. doi:https://doi.org/10.1002/adma.201305506

Komaya, K., Ebata, T., Yokoyama, Y., Igami, T., Sugawara, G., Mizuno, T., . . . Nagino, M. (2018). Recurrence after curative-intent resection of perihilar cholangiocarcinoma: analysis of a large cohort with a close postoperative follow-up approach. *Surgery, 163*(4), 732-738.

Kühlbach, C., Da Luz, S., Baganz, F., Hass, V. C., & Mueller, M. M. (2018). A microfluidic system for the investigation of tumor cell extravasation. *Bioengineering, 5*(2), 40.

Kumar, H., & Kim, K. (2020). Stereolithography 3D Bioprinting (Vol. 2140, pp. 93-108).

Lee, S., Burner, D. N., Mendoza, T. R., Muldong, M. T., Arreola, C., Wu, C. N., . . . Jamieson, C. A. (2020). Establishment and analysis of three-dimensional (3D) organoids derived from patient prostate cancer bone metastasis specimens and their xenografts. *J. Vis. Exp, 156*, e60367.

Lei, M., & Wang, X. (2016). Biodegradable Polymers and Stem Cells for Bioprinting. *Molecules, 21*.

Li, J., Chen, M., Fan, X., & Zhou, H. (2016). Recent advances in bioprinting techniques: approaches, applications and future prospects. *Journal of Translational Medicine, 14*(1), 271. doi:10.1186/s12967-016-1028-0

Li, X., Liu, B., Pei, B., Chen, J., Zhou, D., Peng, J., . . . Xu, T. (2020). Inkjet Bioprinting of Biomaterials. *Chemical reviews, 120*(19), 10793-10833. doi:10.1021/acs.chemrev.0c00008

Lim, K. S., Levato, R., Costa, P. F., Castilho, M. D., Alcala-Orozco, C. R., van Dorenmalen, K. M. A., . . . Woodfield, T. B. F. (2018). Bio-resin for high resolution lithography-based biofabrication of complex cell-laden constructs. *Biofabrication, 10*(3), 034101. doi:10.1088/1758-5090/aac00c

Lindnér, P., Rizell, M., & Hafström, L. (2015). The impact of changed strategies for patients with cholangiocarcinoma in this millenium. *HPB Surgery, 2015*.

Liu, X.-F., Zhang, H., Zhu, S.-G., Zhou, X.-T., Su, H.-L., Xu, Z., & Li, S.-J. (2006). Correlation of p53 gene mutation and expression of P53 protein in cholangiocarcinoma. *World journal of gastroenterology, 12*(29), 4706-4709. doi:10.3748/wjg.v12.i29.4706

Loai, S., Kingston, B. R., Wang, Z., Philpott, D. N., Tao, M., & Cheng, H.-L. M. (2019). Clinical Perspectives on 3D Bioprinting Paradigms for Regenerative Medicine. *Regenerative Medicine Frontiers, 1*(1), e190004. doi:10.20900/rmf20190004

Loessner, D., Meinert, C., Kaemmerer, E., Martine, L. C., Yue, K., Levett, P. A., . . . Hutmacher, D. W. (2016). Functionalization, preparation and use of cell-laden gelatin methacryloyl–based hydrogels as modular tissue culture platforms. *Nature protocols, 11*(4), 727.

Malda, J., Visser, J., Melchels, F. P., Jüngst, T., Hennink, W. E., Dhert, W. J. A., . . . Hutmacher, D. W. (2013). 25th Anniversary Article: Engineering Hydrogels for Biofabrication. *Advanced Materials, 25*(36), 5011-5028. doi:https://doi.org/10.1002/adma.201302042

Matlashewski, G., Lamb, P., Pim, D., Peacock, J., Crawford, L., & Benchimol, S. (1984). Isolation and characterization of a human p53 cDNA clone: expression of the human p53 gene. *The EMBO journal, 3*(13), 3257-3262.

Meacham, C. E., & Morrison, S. J. (2013). Tumour heterogeneity and cancer cell plasticity. *Nature, 501*(7467), 328-337.

Mi, S., Du, Z., Xu, Y., Wu, Z., Qian, X., Zhang, M., & Sun, W. (2016). Microfluidic co-culture system for cancer migratory analysis and anti-metastatic drugs screening. *Scientific Reports, 6*, 35544.

Miao, S., Zhu, W., Castro, N. J., Nowicki, M., Zhou, X., Cui, H., . . . Zhang, L. G. (2016). 4D printing smart biomedical scaffolds with novel soybean oil epoxidized acrylate. *Scientific Reports, 6*, 27226-27226. doi:10.1038/srep27226

Mingaleeva, R., Solovieva, V., Blatt, N., & Rizvanov, A. (2013). Application of cell and tissue cultures for potential anti-cancer/oncology drugs screening in vitro. *Cellular Transplantation & Tissue Engineering, 8*(2).

Mobaraki, M., Ghaffari, M., Yazdanpanah, A., Luo, Y., & Mills, D. K. (2020). Bioinks and bioprinting: A focused review. *Bioprinting, 18*, e00080. doi:https://doi.org/10.1016/j.bprint.2020.e00080

Mueller, S., & Sandrin, L. (2010). Liver stiffness: a novel parameter for the diagnosis of liver disease. *Hepatic medicine : evidence and research, 2*, 49-67. doi:10.2147/hmer.s7394

Munoz-Garrido, P., & Rodrigues, P. M. (2019). The jigsaw of dual hepatocellular–intrahepatic cholangiocarcinoma tumours. *Nature Reviews Gastroenterology & Hepatology*, 1.

Murphy, S. V., & Atala, A. (2014). 3D bioprinting of tissues and organs. *Nat Biotechnol, 32*(8), 773-785.

Nagai, H., & Kim, Y. H. (2017). Cancer prevention from the perspective of global cancer burden patterns. *Journal of thoracic disease, 9*(3), 448-451. doi:10.21037/jtd.2017.02.75

Nakatsu, N., Nakamura, T., Yamazaki, K., Sadahiro, S., Makuuchi, H., Kanno, J., & Yamori, T. (2007). Evaluation of action mechanisms of toxic chemicals using JFCR39, a panel of human cancer cell lines. *Molecular Pharmacology, 72*(5), 1171-1180.

Nakeeb, A., Pitt, H. A., Sohn, T. A., Coleman, J., Abrams, R. A., Piantadosi, S., . . . Cameron, J. L. (1996). Cholangiocarcinoma. A spectrum of intrahepatic, perihilar, and distal tumors. *Annals of surgery, 224*(4), 463.

Nelson, S. R., Zhang, C., Roche, S., O'Neill, F., Swan, N., Luo, Y., . . . Walsh, N. (2020). Modelling of pancreatic cancer biology: transcriptomic signature for 3D PDX-derived organoids and primary cell line organoid development. *Scientific Reports, 10*(1), 1-12.

Ning, L., & Chen, X. (2017). A brief review of extrusion-based tissue scaffold bio-printing. *Biotechnol J, 12*(8), 1600671. doi:https://doi.org/10.1002/biot.201600671

Nishiyama, Y., Nakamura, M., Henmi, C., Yamaguchi, K., Mochizuki, S., Nakagawa, H., & Takiura, K. (2009). Development of a Three-Dimensional Bioprinter: Construction of Cell Supporting Structures Using Hydrogel and State-of-the-Art Inkjet Technology. *J. Biomech. Eng., 131*, 035001.

Oliver, A. J., Lau, P. K. H., Unsworth, A. S., Loi, S., Darcy, P. K., Kershaw, M. H., & Slaney, C. Y. (2018). Tissue-Dependent Tumor Microenvironments and Their Impact on Immunotherapy Responses. *Frontiers in immunology, 9*, 70-70. doi:10.3389/fimmu.2018.00070

Osswald, A., Hedrich, V., & Sommergruber, W. (2019). 3D-3 tumor models in drug discovery for analysis of immune cell infiltration *Target Identification and Validation in Drug Discovery* (pp. 151-162): Springer.

Ozbolat, I. T., & Yu, Y. (2013). Bioprinting toward organ fabrication: challenges and future trends. *IEEE Transactions on Biomedical Engineering, 60*(3), 691-699.

Park, J. H., Jang, J., Lee, J. S., & Cho, D. W. (2017). Three-Dimensional Printing of Tissue/Organ Analogues Containing Living Cells. *Ann Biomed Eng, 45*(1), 180-194. doi:10.1007/s10439-016-1611-9

Park, K. M., Lewis, D., & Gerecht, S. (2017). Bioinspired Hydrogels to Engineer Cancer Microenvironments. *Annual review of biomedical engineering, 19*, 109-133. doi:10.1146/annurev-bioeng-071516-044619

Parkin, D. M. (2006). The global health burden of infection-associated cancers in the year 2002. *International journal of cancer, 118*(12), 3030-3044.

Pepelanova, I., Kruppa, K., Scheper, T., & Lavrentieva, A. (2018). Gelatin-Methacryloyl (GelMA) Hydrogels with Defined Degree of Functionalization as a Versatile Toolkit for 3D Cell Culture and Extrusion Bioprinting. *Bioengineering (Basel, Switzerland), 5*(3), 55. doi:10.3390/bioengineering5030055

Pereira, R. F., & Bártolo, P. J. (2015). 3D bioprinting of photocrosslinkable hydrogel constructs. *Journal of Applied Polymer Science, 132*(48). doi:https://doi.org/10.1002/app.42458

Petta, D., Armiento, A. R., Grijpma, D., Alini, M., Eglin, D., & D'Este, M. (2018). 3D bioprinting of a hyaluronan bioink through enzymatic-and visible light-crosslinking. *Biofabrication, 10*(4), 044104. doi:10.1088/1758-5090/aadf58

Poologasundarampillai, G., & Nommeots-Nomm, A. (2017). 3 - Materials for 3D printing in medicine: Metals, polymers, ceramics, hydrogels. In D. M. Kalaskar (Ed.), *3D Printing in Medicine* (pp. 43-71): Woodhead Publishing.

Poon, S. L., McPherson, J. R., Tan, P., Teh, B. T., & Rozen, S. G. (2014). Mutation signatures of carcinogen exposure: genome-wide detection and new opportunities for cancer prevention. *Genome medicine, 6*(3), 24.

Puls, T., Tan, X., Husain, M., Whittington, C. F., Fishel, M. L., & Voytik-Harbin, S. L. (2018). Development of a novel 3D tumor-tissue invasion model for high-throughput, high-content phenotypic drug screening. *Scientific Reports, 8*(1), 1-14.

Qingyi, W., & Lei, L. (2007). *DNA repair, genetic instability, and cancer*: World scientific.

Raman, R., & Bashir, R. (2015). Chapter 6 - Stereolithographic 3D Bioprinting for Biomedical Applications. In A. Atala & J. J. Yoo (Eds.), *Essentials of 3D Biofabrication and Translation* (pp. 89-121). Boston: Academic Press.

Rayleigh, L. (1878). On the Instability of Jets. *Proceedings of the London Mathematical Society, S1-10*, 4.

Rayleigh, L. (1891). Some Applications of Photography1. *Nature, 44*, 249.

Raza, F., Zafar, H., Zhu, Y., Ren, Y., Ullah, A., Khan, A. U., . . . Ge, L. (2018). A Review on Recent Advances in Stabilizing Peptides/Proteins upon Fabrication in Hydrogels from Biodegradable Polymers. *Pharmaceutics, 10*(1). doi:10.3390/pharmaceutics10010016

Rees, A., Powell, L. C., Chinga-Carrasco, G., Gethin, D. T., Syverud, K., Hill, K. E., & Thomas, D. W. (2015). 3D Bioprinting of Carboxymethylated-Periodate Oxidized Nanocellulose Constructs for Wound Dressing Applications. *Biomed Res Int, 2015*, 925757. doi:10.1155/2015/925757

Riedl, A., Schlederer, M., Pudelko, K., Stadler, M., Walter, S., Unterleuthner, D., . . . Kenner, L. (2017). Comparison of cancer cells in 2D vs 3D culture reveals differences in AKT–mTOR–S6K signaling and drug responses. *Journal of Cell Science, 130*(1), 203-218.

Rimann, M., Bono, E., Annaheim, H., Bleisch, M., & Graf-Hausner, U. (2016). Standardized 3D Bioprinting of Soft Tissue Models with Human Primary Cells. *J Lab Autom, 21*(4), 496-509. doi:10.1177/2211068214567146

Rizvanov, A. A., Yalvaç, M. E., Shafigullina, A. K., Salafutdinov, I. I., Blatt, N. L., Sahin, F., . . . Palotás, A. (2010). Interaction and self-organization of human mesenchymal stem cells and neuro-blastoma SH-SY5Y cells under co-culture conditions: A novel system for modeling cancer cell micro-environment. *European journal of pharmaceutics and biopharmaceutics, 76*(2), 253-259.

Rizvi, S., Khan, S. A., Hallemeier, C. L., Kelley, R. K., & Gores, G. J. (2018). Cholangiocarcinoma—evolving concepts and therapeutic strategies. *Nature reviews Clinical oncology, 15*(2), 95.

Ruedinger, F., Lavrentieva, A., Blume, C., Pepelanova, I., & Scheper, T. (2015). Hydrogels for 3D mammalian cell culture: a starting guide for laboratory practice. *Applied microbiology and biotechnology, 99*(2), 623-636.

Ruzycka, M., Cimpan, M. R., Rios-Mondragon, I., & Grudzinski, I. P. (2019). Microfluidics for studying metastatic patterns of lung cancer. *Journal of Nanobiotechnology, 17*(1), 71.

Saunders, R. E., & Derby, B. (2014). Inkjet printing biomaterials for tissue engineering: bioprinting. *International Materials Reviews, 59*(8), 430-448.

Schacht, K., Jüngst, T., Schweinlin, M., Ewald, A., Groll, J., & Scheibel, T. (2015). Biofabrication of Cell-Loaded 3D Spider Silk Constructs. *Angewandte Chemie International Edition, 54*(9), 2816-2820. doi:https://doi.org/10.1002/anie.201409846

Schneider, J. M., & Hendricks, C. D. (1964). Source of Uniform-Sized Liquid Droplets. *Rev. Sci. Instrum., 35*, 1349.

Schottenfeld, D., & Fraumeni Jr, J. F. (2006). *Cancer epidemiology and prevention*: Oxford University Press.

Seidi, K., Neubauer, H. A., Moriggl, R., Jahanban-Esfahlan, R., & Javaheri, T. (2018). Tumor target amplification: implications for nano drug delivery systems. *Journal of Controlled Release, 275*, 142-161.

Seto, M., Honma, K., & Nakagawa, M. (2010). Diversity of genome profiles in malignant lymphoma. *Cancer science, 101*(3), 573-578.

Shoemaker, R. H. (2006). The NCI60 human tumour cell line anticancer drug screen. *Nature Reviews Cancer, 6*(10), 813-823.

Shtivelman, E., Lifshitz, B., Gale, R. P., & Canaani, E. (1985). Fused transcript of abl and bcr genes in chronic myelogenous leukaemia. *Nature, 315*(6020), 550-554.

Siegel, R., Naishadham, D., & Jemal, A. (2013). Cancer statistics, 2013. *CA Cancer J Clin, 63*(1), 11-30. doi:10.3322/caac.21166

Siegel, R. L., Miller, K. D., & Jemal, A. (2016). Cancer statistics, 2016. *CA Cancer J Clin, 66*(1), 7-30. doi:10.3322/caac.21332

Singh, M., Haverinen, H. M., Dhagat, P., & Jabbour, G. E. (2010). Inkjet Printing—Process and Its Applications. *Advanced Materials, 22*(6), 673-685. doi:https://doi.org/10.1002/adma.200901141

Sinha, R. P., & Häder, D.-P. (2002). UV-induced DNA damage and repair: a review. *Photochemical & Photobiological Sciences, 1*(4), 225-236.

Skardal, A., Devarasetty, M., Kang, H.-W., Mead, I., Bishop, C., Shupe, T., . . . Atala, A. (2015). A hydrogel bioink toolkit for mimicking native tissue biochemical and mechanical properties in bioprinted tissue constructs. *Acta Biomaterialia, 25*, 24-34. doi:https://doi.org/10.1016/j.actbio.2015.07.030

Skoog, S. A., Goering, P. L., & Narayan, R. J. (2014). Stereolithography in tissue engineering. *J Mater Sci Mater Med, 25*(3), 845-856. doi:10.1007/s10856-013-5107-y

Sleeboom, J. J., Amirabadi, H. E., Nair, P., Sahlgren, C. M., & Den Toonder, J. M. (2018). Metastasis in context: modeling the tumor microenvironment with cancer-on-a-chip approaches. *Disease models & mechanisms, 11*(3).

Sounni, N. E., & Noel, A. (2013). Targeting the tumor microenvironment for cancer therapy. *Clin Chem, 59*(1), 85-93.

Stansbury, J. W., & Idacavage, M. J. (2016). 3D printing with polymers: Challenges among expanding options and opportunities. *Dent Mater, 32*(1), 54-64. doi:10.1016/j.dental.2015.09.018

Stevens, J. L., & Baker, T. K. (2009). The future of drug safety testing: expanding the view and narrowing the focus. *Drug discovery today, 14*(3-4), 162-167.

Stock, K., Estrada, M. F., Vidic, S., Gjerde, K., Rudisch, A., Santo, V. E., . . . Graeser, R. (2016). Capturing tumor complexity in vitro: Comparative analysis of 2D and 3D tumor models for drug discovery. *Scientific Reports, 6*(1), 28951. doi:10.1038/srep28951

Strijker, M., Belkouz, A., van der Geest, L. G., van Gulik, T. M., van Hooft, J. E., de Meijer, V. E., . . . de Vos-Geelen, J. (2019). Treatment and survival of resected and unresected distal cholangiocarcinoma: a nationwide study. *Acta Oncologica, 58*(7), 1048-1055.

Sweet, R. G. (1965). High Frequency Recording with Electrostatically Deflected Ink Jets. *Rev. Sci. Instrum., 36*, 131.

Takimoto, C. H. (2003). Anticancer drug development at the US National Cancer Institute. *Cancer chemotherapy and pharmacology, 52*(1), 29-33.

Teicher, B. A. (2010). *Tumor models in cancer research*: Springer Science & Business Media.

Thomas, B. H., Craig Fryman, J., Liu, K., & Mason, J. (2009). Hydrophilic–hydrophobic hydrogels for cartilage replacement. *Journal of the Mechanical Behavior of Biomedical Materials, 2*(6), 588-595. doi:https://doi.org/10.1016/j.jmbbm.2008.08.001

Trafialek, J., & Kolanowski, W. (2014). Dietary exposure to meat-related carcinogenic substances: is there a way to estimate the risk? *International journal of food sciences and nutrition, 65*(6), 774-780.

Uchida, Y., Tanaka, S., Aihara, A., Adikrisna, R., Yoshitake, K., Matsumura, S., . . . Irie, T. (2010). Analogy between sphere forming ability and stemness of human hepatoma cells. *Oncology reports, 24*(5), 1147-1151.

Valkenaers, H., Vogeler, F., Voet, A., & Kruth, J. (2013). *Screw extrusion based 3D printing, a novel additive manufacturing technology*.

Van Den Bulcke, A. I., Bogdanov, B., De Rooze, N., Schacht, E. H., Cornelissen, M., & Berghmans, H. (2000). Structural and rheological properties of methacrylamide modified gelatin hydrogels. *Biomacromolecules, 1*(1), 31-38.

Vantangoli, M., Madnick, S., Huse, S., Weston, P., & Boekelheide, K. (2015). MCF-7 Human Breast Cancer Cells Form Differentiated Microtissues in Scaffold-Free Hydrogels. *PLoS ONE, 10*, e0135426. doi:10.1371/journal.pone.0135426

Wan, L., Neumann, C. A., & LeDuc, P. R. (2020). Tumor-on-a-chip for integrating a 3D tumor microenvironment: chemical and mechanical factors. *Lab on a Chip, 20*(5), 873-888. doi:10.1039/C9LC00550A

Wang, S., Li, E., Gao, Y., Wang, Y., Guo, Z., He, J., . . . Wang, Q. (2013). Study on invadopodia formation for lung carcinoma invasion with a microfluidic 3D culture device. *PLoS ONE, 8*(2), e56448.

Wood, R. D., Mitchell, M., & Lindahl, T. (2005). Human DNA repair genes, 2005. *Mutation Research/Fundamental and Molecular Mechanisms of Mutagenesis, 577*(1-2), 275-283.

Wu, G.-H., & Hsu, S.-H. (2015). Review: Polymeric-Based 3D Printing for Tissue Engineering. *Journal of medical and biological engineering, 35*(3), 285-292. doi:10.1007/s40846-015-0038-3

Wu, Z., Su, X., Xu, Y., Kong, B., Sun, W., & Mi, S. (2016). Bioprinting three-dimensional cell-laden tissue constructs with controllable degradation. *Scientific Reports, 6*(1), 24474. doi:10.1038/srep24474

Xu, T., Baicu, C., Aho, M., Zile, M., & Boland, T. (2009). Fabrication and characterization of bio-engineered cardiac pseudo tissues. *Biofabrication, 1*(3), 035001.

Yoo, K. Y., & Shin, H. R. (2003). Cancer epidemiology and prevention. *Korean Journal of Epidemiology, 25*(1), 1-15.

Yoon, H., Shin, S., Cha, J., Lee, S.-H., Kim, J.-H., Do, J. T., . . . Bae, H. (2016). Cold Water Fish Gelatin Methacryloyl Hydrogel for Tissue Engineering Application. *PLoS ONE, 11*, e0163902. doi:10.1371/journal.pone.0163902

You, F., Eames, B. F., & Chen, X. (2017). Application of Extrusion-Based Hydrogel Bioprinting for Cartilage Tissue Engineering. *International Journal of Molecular Sciences, 18*(7), 1597. doi:10.3390/ijms18071597

Yu, Y., & Ozbolat, I. T. (2014, 26-30 Aug. 2014). *Tissue strands as "bioink" for scale-up organ printing.* Paper presented at the 2014 36th Annual International Conference of the IEEE Engineering in Medicine and Biology Society.

Yue, K., Trujillo-de Santiago, G., Alvarez, M. M., Tamayol, A., Annabi, N., & Khademhosseini, A. (2015). Synthesis, properties, and biomedical applications of gelatin methacryloyl (GelMA) hydrogels. *Biomaterials, 73*, 254-271. doi:https://doi.org/10.1016/j.biomaterials.2015.08.045

Zheng, Z., Eglin, D., Alini, M., Richards, G. R., Qin, L., & Lai, Y. (2020). Visible Light-Induced 3D Bioprinting Technologies and Corresponding Bioink Materials for Tissue Engineering: A Review. *Engineering*. doi:https://doi.org/10.1016/j.eng.2020.05.021

Zhu, M., Wang, Y., Ferracci, G., Zheng, J., Cho, N.-J., & Lee, B. H. (2019). Gelatin methacryloyl and its hydrogels with an exceptional degree of controllability and batch-to-batch consistency. *Scientific Reports, 9*(1), 6863. doi:10.1038/s41598-019-42186-x

Zhu, W., Wang, M., Fu, Y., Castro, N. J., Fu, S. W., & Zhang, L. G. (2015). Engineering a biomimetic three-dimensional nanostructured bone model for breast cancer bone metastasis study. *Acta Biomater, 14*, 164-174. doi:10.1016/j.actbio.2014.12.008

Zongjie, W., Abdulla, R., & Parker, B. (2015). A simple and high-resolution stereolithography-based 3D bioprinting system using visible light crosslinkable bioinks. Biofabrication, 7 (4): 045009: ed.

Zorlutuna, P., Annabi, N., Camci-Unal, G., Nikkhah, M., Cha, J. M., Nichol, J. W., . . . Khademhosseini, A. (2012). Microfabricated biomaterials for engineering 3D tissues. *Adv Mater, 24*(14), 1782-1804. doi:10.1002/adma.201104631

## Acknowledgements

My time in the Laboratory of Yu Shrike Zhang at the Harvard Medical School was educational from a methodical, as well as a theoretical point of view. Additionally, did my internship abroad enhance many personal skills. Therefore, in my opinion, it will be beneficial for my future career and me personally.

Taking this opportunity, I would like to express appreciation to my supervisor and head of the laboratory Yu Shrike Zhang, PhD. Thank you for granting me the possibility of doing my Master thesis within your laboratory. It was a pleasure working with the people in your laboratory.

Also, many thanks to Qiong, Santiago and Cesar, it was great working with you. In particular, I am very thankful for you three always having an open ear for when I had questions and needed help.

I am also appreciative for the Marshall Plan Foundation's financial support and Dr Zhanial for her guidance.

I am grateful for the support of my family and friends, especially during these uncertain times. Most of all, my wife, it was great experiencing this time, but it was even greater experiencing it with you. I am looking forward to even more adventures with you together in the future.

*Erklärung:*

*Ich erkläre, dass die vorliegende Diplomarbeit/Masterarbeit von mir selbst verfasst wurde und ich keine anderen als die angeführten Behelfe verwendet bzw. mich auch sonst keiner unerlaubter Hilfe bedient habe.*

*Ich versichere, dass ich diese Diplomarbeit/Masterarbeit bisher weder im In- noch im Ausland (einer Beurteilerin/einem Beurteiler zur Begutachtung) in irgendeiner Form als Prüfungsarbeit vorgelegt habe.*

*Weiters versichere ich, dass die von mir eingereichten Exemplare (ausgedruckt und elektronisch) identisch sind.*

Declaration:

I hereby declare that the submitted Master thesis was written by myself and that I did not use any aids other than those indicated, none of which are unauthorised.

I assure that I have not previously submitted this Master thesis or its contents in any form for assessment as part of an examination either in Austria or abroad.

Furthermore, I assure that all copies submitted by myself (electronic and printed) are identical.

Date: 17.2.2021 Signature: .....

# Appendix

## Appendix I – Figure Licenses

Permissions and licenses were obtained for every figure used in this thesis. A list of said licenses can be found below:

**Figure 1**

The figure was obtained from (Jesus M. Banales et al., 2020) which is licensed under Creative Commons Version 4.0 CC BY which can be found at http://creativecommons.org/licenses/by/4.0/ .

**Figure 2**

The figure was obtained from (Jesus M. Banales et al., 2020) which is licensed under Creative Commons Version 4.0 CC BY which can be found at http://creativecommons.org/licenses/by/4.0/.

China was replaced by Mainland China.

**Figure 3**

The figure was obtained from (Alsibai & Meseure, 2018) which is licensed under Creative Commons Version 3.0 CC BY which can be found at https://creativecommons.org/licenses/by/3.0/ .

**Figure 4**

The figure was obtained from (Kristina V. Kitaeva et al., 2020) which is licensed under Creative Commons Version 4.0 CC BY which can be found at https://creativecommons.org/licenses/by/4.0/ .

**Figure 5**

Reprinted by permission from John Wiley and Sons: Journal of Applied Polymer Science /Volume 132, Issue 48 “3D bioprinting of photocrosslinkable hydrogel constructs” by Rúben F. Pereira and Paulo J. Bártolo

| | |
|---|---|
| License Number | 5006730359195 |
| License Date | Feb 12, 2021 |
| Licensed Content Publisher | John Wiley and Sons |
| Licensed Content Publication | Journal of Applied Polymer |
| Licensed Content Title | 3D bioprinting of photocrosslinkable hydrogel constructs |
| Licensed Content Author | Rúben F. Pereira and Paulo J. Bártolo |
| Licensed Content Date | July 21, 2015 |

**Figure 6**

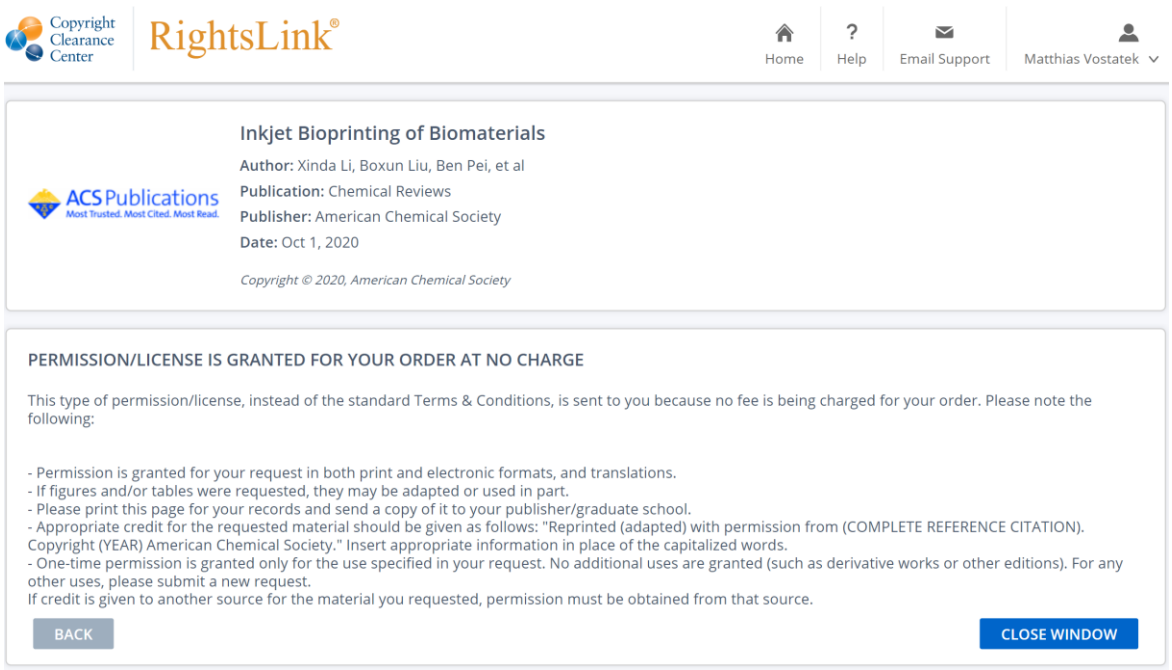


Permission for this figure was requested and granted on February 13, 2021

**Figure 7**

The figure was obtained from (Jang, 2017) which is licensed under Creative Commons Version 4.0 CC BY which can be found at https://creativecommons.org/licenses/by/4.0/ .

**Figure 8**

The figure was obtained from (Jang, 2017) which is licensed under Creative Commons Version 4.0 CC BY which can be found at https://creativecommons.org/licenses/by/4.0/ .

**Figure 9**

The figure was obtained from (Loai et al., 2019) which is licensed under Creative Commons Version 4.0 CC BY which can be found at https://creativecommons.org/licenses/by/4.0/ .

**Figure 10**

The figure was obtained from (Yoon et al., 2016) which is licensed under Creative Commons Version 4.0 CC BY which can be found at https://creativecommons.org/licenses/by/4.0/ .